REPORT DOCUMENTATION PAGE

Form Approved
OMB No 0704-0188
Exp Date Jun 30, 1986

1a. REPORT SECURITY CLASSIFICATION Unclassified	1b. RESTRICTIVE MARKINGS
2a. SECURITY CLASSIFICATION AUTHORITY	3. DISTRIBUTION/AVAILABILITY OF REPORT Approved for public release; distribution unlimited
2b. DECLASSIFICATION/DOWNGRADING SCHEDULE	
4. PERFORMING ORGANIZATION REPORT NUMBER(S)	5. MONITORING ORGANIZATION REPORT NUMBER(S) R&D 5909-MS-01
6a. NAME OF PERFORMING ORGANIZATION University of Cambridge 6b. OFFICE SYMBOL (If applicable)	7a. NAME OF MONITORING ORGANIZATION European Research Office USARDSG-UK
6c. ADDRESS (City, State, and ZIP Code) Madingley Road Cambridge, CB3 0HE	7b. ADDRESS (City, State, and ZIP Code) Box 65 FPO NY 09510-1500
8a. NAME OF FUNDING/SPONSORING ORGANIZATION European Research Office USARDSG-UK ARO-E 8b. OFFICE SYMBOL (If applicable)	9. PROCUREMENT INSTRUMENT IDENTIFICATION NUMBER DAJA45-87-C-0059
8c. ADDRESS (City, State, and ZIP Code) Box 65 FPO NY 09510-1500	10. SOURCE OF FUNDING NUMBERS PROGRAM ELEMENT NO. 61102A; PROJECT NO. 1L161102BH57; TASK NO. 04; WORK UNIT ACCESSION NO
11. TITLE (Include Security Classification) (U) Processing of Mixed Oxide Superconductors	
12. PERSONAL AUTHOR(S) Dr. A.M. Campbell and Professor M.F. Ashby	
13a. TYPE OF REPORT Final	13b. TIME COVERED FROM 12.87 TO 7.90
14. DATE OF REPORT (Year, Month, Day) 90.07	15. PAGE COUNT 37
16. SUPPLEMENTARY NOTATION	

17. COSATI CODES		
FIELD	GROUP	SUB-GROUP
11	02	
20	12	

18. SUBJECT TERMS (Continue on reverse if necessary and identify by block number)
High Temperature Superconductivity, critical current superconductor, ceramic, magnetism

19. ABSTRACT (Continue on reverse if necessary and identify by block number)

This work was initiated soon after the discovery of high temperature superconductors. Although much effort was being put into the research for higher temperature materials, it rapidly became clear that the main obstacle to the application of these materials was the low critical current density. Although in conventional materials the critical current density was determined by the pinning of flux lines by defects in the microstructure in high Tc materials, the appearance of weak links, or Josephson Junctions, at grain boundaries was the dominant effect. This was a completely new phenomena and led not only to rather low critical current densities in zero field but to a catastrophic drop in fields of only a few millitesla, although the upper critical field of these materials is extremely high (probably greater than 150 Tesla). The work can be divided into four main sections. These are magnetic separation, levitation, screening, and critical current studies. Each has led to several publications or internal reports which are part of this report.

(TTL)

20. DISTRIBUTION/AVAILABILITY OF ABSTRACT ☒ UNCLASSIFIED/UNLIMITED ☐ SAME AS RPT. ☒ DTIC USERS	21. ABSTRACT SECURITY CLASSIFICATION Unclassified
22a. NAME OF RESPONSIBLE INDIVIDUAL Dr. Wilbur C. Simmons	22b. TELEPHONE (Include Area Code) 071-409 4423/4485 22c. OFFICE SYMBOL AMXSN-UK-RM

DD FORM 1473, 84 MAR

83 APR edition may be used until exhausted.
All other editions are obsolete.

SECURITY CLASSIFICATION OF THIS PAGE
Unclassified

2

Contract DAJA45-87-C-0059

Processing of Mixed Oxide Superconductors

A.M.Campbell and M.F.Ashby

University of Cambridge.

Final Report

Final Report on Contract DAJA45-87-C-0059,
'Processing of Mixed Oxide Superconductors'

Introduction

This work was initiated soon after the discovery of high temperature superconductors. Although much effort was being put into the search for higher temperature materials, it rapidly became clear that the main obstacle to the application of these materials was the low critical current density. Although in conventional materials the critical current density was determined by the pinning of flux lines by defects in the microstructure in high T_c materials the appearance of weak links, or Josephson Junctions, at grain boundaries was the dominant effect. This was a completely new phenomenon and led not only to rather low critical current densities in zero field but to a catastrophic drop in fields of only a few millitesla, although the upper critical field of these materials is extremely high (probably greater than 150 Tesla). Since artificial weak links are the basis of most electronic applications of superconductors their appearance at natural grain boundaries suggested that it would be extremely difficult to use conventional techniques to make devices and this has proved to be the case. Understanding and control of the weak links at grain boundaries was clearly the key to applications of the high Tc materials and this still remains true. This contract was initiated at an early stage in this subject, which developed at an unprecedented rate and a number of different lines have been tackled in the course of the last two years. In addition to rapid changes world wide a major research centre on high Tc superconductors was awarded to Cambridge which involved moving the work and people to a new site and the creation of a large new laboratory containing physicists, materials scientists, chemists and engineers. Although in the long term this makes for a much more powerful group it inevitably led to considerable disruption in the middle stages of this project. The work can be divided into four main sections. These are magnetic separation, levitation, screening, and critical current studies. Each has led to several publications or internal reports which are enclosed as part of this report. The sections which follow summarise the main conclusions of these papers, the main text of these reports and paper is in the appendices.

Separation

Ceramic superconductors tend to be mixtures of phases, especially when first discovered. It would be very useful to separate out the superconducting from the non superconducting phases so that they could be studied on their own. The diamagnetic properties of the superconducting state will in principle allow superconducting material to be levitated from the non superconductor and several designs of separator were tested. There are a number of difficulties which emerged.

1) It was essential to allow time for the particles to come to the right temperature. This meant that dropping particles, even in a liquid, was unsatisfactory unless they were held for a time at a low temperature.
2) Electrostatic forces on fine powders are very strong so that it was difficult to avoid clumping and sticking to substrates.
3)To get large forces we need a large field gradient, but fields less than H_{c1}. This is very low in high T_c materials and if exceeded leads to paramagnetic moments as the field decreases so that the graph of force against distance from the magnet is very complex.
4)Turbulence causes normal particles to scatter instead of falling vertically.
5)Materials with the highest T_c appear to be layer structures with a very large penetration depth in one direction. Particles turn so that the magnetisation is a minimum and so small particles of these materials do not levitate.

The first experiments used a dry system with the powder vibrated on a solid sheet (Appendix I). This has a major advantage in bringing the particles to temperature slowly and does not require actual levitation. However clumping and sticking of particles led to unsatisfactory operation.

The most successful apparatus is described in Appendix II. There are two versions, one for small quantities and one for larger scale separation. Material was brought to temperature in liquid nitrogen and dropped through a sieve onto a conical magnet with a hole in its centre. This worked well in separating YBCO from non superconducting material. The main error was some scattered normal material being deflected outside the central hole. Further development would require the technique to be extended to a wide range of temperature. Gas would be used instead of liquid and the both dropper and collector would have to be put in a container with accurate and uniform temperature control. This is quite feasible but was not attempted within the time scale of this project. Before embarking on it it would be necessary to measure the levitating properties of a number of materials since it appears that YBCO is unusually easy to levitate because of its relatively small penetration depth.

Levitation and Damping

The study of forces on particles gave a better understanding of the levitation process and A.C. measurements described below are a measure of the frictional forces. It seemed a useful idea to put these together and see if the damping of a levitated magnet could be explained quantitatively. In general moving and rotating magnets cause large field fluctuations and the resulting hysteresis losses bring it to rest fairly quickly. However if a magnet rotates about its axis of symmetry the field should be constant and there should be no damping. Gyroscopes using superconducting niobium have extremely low damping and it would be very useful to make a similar machine of high T_c material. The results are in Appendix III. The geometry used was a disc floating above a sintered sheet of YBCO. The magnet was set rotating about its centre and the time to come to rest measured. Although damping was much less than in other modes, typical times of the order of twenty or thirty seconds meant that the performance was well below that found in niobium. To determine the reasons a magnetic map of the magnet was made with a search coil. It was found that there were field fluctuations of the order of a few millitesla due to magnet inhomogeneity and considerably larger ones due to a small chip in the magnet edge. At the height at which the magnet was levitating the field at the superconductor was well above H_{c1} so that losses will be relatively high and the observed values were consistent with the damping of the magnet. There are two ways of improving the performance of this bearing. One is to improve the magnet homogeneity, the other to increase the critical current density of the superconductor. Improving J_c will also give a much stiffer bearing, or a greater height of levitation, so we can expect greatly decreased damping as materials improve.

Screening and Flux Trapping.

It was clear from an early stage that there were two separate critical current densities in high T_c materials, the intergrain currents between grains and the intra grain currents within them. These differ by three orders of magnitude and it is important to be able to measure both. The first technique developed was to measure the fields inside and outside a hollow cylinder. The experimental results showed that a significant field was being generated by the diamagnetism of the grains and that this, combined with self field effects, made most of the current flow on the outer surface when field was trapped in the cylinder.(Appendix IV) The method was superseded by an A.C. technique described below which did not require hollow cylinders, but it led to an interest in the screening properties of high T_c ceramics. A theoretical calculation showed that screening due to diamagnetic particles without supercurrents between them was only effective close to the screen. (Appendix V) This explains why a ceramic can levitate a magnet which is close to it but is not good at screening fields at large distances compared with its thickness. To provide good screening for any but the lowest fields a high critical current density is required.

Critical Current Studies

The central problem was (and remains) the weak links at grain boundaries. The original intention was to use hot isostatic pressing and standard sintering techniques to consolidate the ceramic. There were clearly going to be problems with oxygen loss and subsequent oxidation but it rapidly became clear that the problem was more fundamental than merely cleaning up the grain boundaries. It was therefore necessary to do some more fundamental work on the nature of the boundaries and why they were causing problems. This decision was clearly the right one since no improvements in sintering techniques have yielded a useful material. The most successful have all involved melting and only small samples have been produced.

Firstly a calculation was made using numerical solutions of the Ginzburg-Landau equations. Although not very accurate we were able to test various hypotheses for the low current densities. None worked very well and in general the results suggest a good deal of damage over many coherence lengths is needed to explain the experimental values. since many boundaries look very clean oxygen loss or crystal relaxation may be the explanation. (Appendix VI)

An A.C. apparatus was developed to measure critical current densities and the penetration of flux into the sample. This was based on our earlier work with conventional superconductors, but the granular nature of high T_c materials meant that the interpretation was not straightforward. The critical current measured is affected by demagnetising factors and the self field of the current. The first is dealt with by plotting results as a function of the internal field. (This is described in Appendix VII) The second shows up as nonlinearity on the flux penetration graph and in many samples the true zero field current would only be measured if the thickness is less than a third of a millimeter. Another new effect is that many samples were much less than fully diamagnetic. Most authors have interpreted this to mean that the sample was not single phase, but we believe that in most cases the true interpretation is that the London penetration depth is comparable with the particle size. In general doping seems to lead to large increases in the penetration depth. Since the calibration of the system depends on knowing how much material is superconducting this effect is important in the interpretation of all magnetic measurements.

The first measurements concentrated on the effect of twins on the critical current within grains. These had been proposed as pinning centers which would increase J_c, or alternatively as weak links which would decrease it. By doping with cobalt to eliminate twins we were able to show that the effect of twins on J_c is generally very small (later work by others has shown a significant pinning effect if the orientation of the field is accurately parallel to the twin planes. We then looked at the effect of cobalt doping on the inter and intragrain critical current densities. The first striking result was that both critical currents decreased in the same proportion. This seems surprising since one is supposed to be limited by

flux pinning within grains and the other by Josephson tunnelling across grain boundaries. These two very different mechanisms and locations would be expected to be affected quite differently by the cobalt. The result suggested that both might be expressed as a proportion of the depairing current, H_c/λ. Measurements of H_{c1} and H_c were made and there was certainly a correlation between the depairing current and the critical currents. However there are considerable uncertainties in these measurements so that a quantitative fit could not be relied on. Using the Abrikosov theory we calculated H_{c2} at zero field from H_{c1} and H_c, since it is much too high to measure directly. This showed that the cobalt was decreasing H_{c2} and therefore increasing the coherence length. Since the critical current was also decreased it is difficult to justify the conventional view that the weak links at grain boundaries are caused by the short coherence length. If this were the case increasing the coherence length should increase the critical current density which is the opposite of what was observed. A preliminary report of these results was given at the MRS meeting in San Francisco this year and they are now being written up for publication.

Conclusions and future work

A reasonably complete understanding of the macroscopic consequences of the granular nature of high Tc materials has been obtained. Levitation, damping, and screening are all consistent with the picture of large intragrain currents and small intergrain currents. Magnetic separation works well for YBCO in liquid nitrogen. The technique can certainly be extended to other materials but foe practical purposes problems may occur due to the large penetration depth and small size of new materials when first prepared. The causes of, and solutions to, the problem of weak links at grain boundaries remain obscure. The work has shown that there is a close link between the intergrain and intragrain currents and that the short coherence length of oxide superconductors is not the main problem. The closest correlation seems to be with the depairing current so that we should look for materials or dopants which decrease the London penetration depth or increase the the thermodynamic critical field. Future work should concentrate on this area and in particular follow up the clues offered by recent excellent results on Bi based superconductors at low temperatures.

Appendix I

Dry Separation

Internal Report by A.Perry

2. Magnetic Separation

Superconductor material is currently used in two forms; it can be made as a thin film on a substrate surface (by ion sputtering, evaporation, etc) or pressed as a powder into molds and sintered into a required shape. The former method is sufficient for applications that only require a thin layer of current transport but many applications require solid items that cannot simply be evaporated as a thin layer onto a shaped surface. In these applications it is necessary to sinter the powder, then to oxygenate the item at elevated temperature to return the oxygen lost during sintering to the crystal structure.

The powder material to be pressed into shape is currently formed from precursors that are usually the oxides or nitrates of the elements involved. These are thoroughly mixed and baked to assist diffusion. The resulting material is ground to a fine powder to mix the resultants as finely as possible and baked again. After a number of such steps the composition is sufficiently uniform for superconductivity to occur. There are a number of ways that the initial mixing stages can be facilitated by using intermediate compound precursors, finer initial powders, mixing in suspension etc. but the basic method remains unchanged.

The resulting powder, ready for pressing to shape, consists of a proportion of material with the correct composition together with quantities of various 'close' compounds that do not have the required properties. When this powder is pressed, the sintered material will consist of regions of useful superconductor connected by bridges between the powder grains. The resulting network of regions is affected by the fraction of other compounds that do not contribute to conduction and reduce the overall cross-section of conductor.

For any given proportion of useful superconductor, centred on the composition value required, the diffusion process that led to its generation will not average the composition between grains, leading to small variations in composition. These can still superconduct, but their properties will be noticably worse than the intended result.

As newer materials are found, many of the better performance materials can form in several different phases of which only one is the improved performance and the others, while useful in their own right, are merely impurities in the required material.

With these considerations in mind, it is clear that some form of grading system is needed to separate a quantity of powder into the various superconducting phases present and to remove the useless material for recycling. If the initial average mixture had the correct composition, then the removal of superconducting (and hence correct composition) material will not affect the mix of the rejected material and this can then be recycled into the next batch to be baked.

Observed powder properties

It is easy to plan simple methods of grading such a material; most prospective schemes fail after some experimentation with the powder.

While on the scale of superconduction the grains of powder can be considered quite large, as a quantity of powder the grains are not distinquishable; like most fine powders they can bind together into clumps that do not easily separate and tend to 'stick' to any surface. It will hence not slide or pour down inclines, but prefer to electrostatically attach itself to the surface and remain where it was placed. Any piece of powder that is willing to move is likely to be a clump which, while large enough to avoid staying in place, can not be graded as the clump will contain a variety of phases.

The force experienced by any superconducting particle in a field is large compared to its weight, but easily overshadowed by air movement or a neighbouring surface. Unless a carrying surface is smooth, the powder is unlikely to move freely. Any liquid nitrogen can push clumps around, especially if floating above a vapour layer, but it does not appear to interact sufficiently with any 'stuck' material that would move it.

Separating forces

For particles of this size range it is easy to show that the forces available by Meissner effects are far too small to be useful and it is necessary to work in higher fields, using the forces due to pinned flux. While we could easily derive the likely forces by using theory and considering a simple sphere of superconductor with some value of critical current and integrating, there is little point in doing so as a measured magnetisation curve for the powder can tell us the parameters we require.

As the ambient magnetic field increases, the reversible magnetisation curve drops to zero and flattens; the energy of the magnetic state of the superconductor, $\mathbf{H}.\mathbf{M_r}$ is virtually unchanged by small changes in the local field intensity. It is hence necessary to use large field intensity gradients to apply reversible forces.

$$\begin{aligned} F_r &= \mathbf{M_r}\frac{d\mathbf{H}}{dx} + \mathbf{H}\frac{d\mathbf{M_r}}{dx} \\ &\approx M_r\frac{d\mathbf{H}}{dx} \end{aligned}$$

Flux pinning forces, on the other hand, manifest themselves as the irreversability of a magnetisation curve. The force required to irreversibly move some material can be found by considering it to be moved back again. As the field changes, the irreversible magnetisation varies as the flux is resisted by the pinning forces and M varies from $M_{dec} = M_r - \delta M$ to $M_{inc} = M_r + \delta M$. The energy dissipated by traversing a loop in the magnetisation diagram is its area; the force resisting motion is thus half the rate of this dissipation of energy with field and distance. For large fluctuations where $\mu_0\mathbf{H} \gg \mathbf{M_r}$ we have

$$\begin{aligned} E_i &= \delta M(H - \delta M/\mu_0) \\ \frac{dE_i}{dH} &\approx \delta M \\ F_i &= \frac{dH}{dx}\frac{dE_i}{dH} = \frac{dH}{dx}\delta M \end{aligned}$$

This is not valid during small field variations, as the loop traversed is no longer an angled parallelogram and collapses into an ellipse. Then

$$\begin{aligned} \delta E &= \frac{4\mu^2}{27\delta M}\delta H^3 \\ \frac{dE_i}{dH} &= \frac{4\mu^2}{9\delta M}\delta H^2 \\ F_i &= \frac{4\delta B^2}{9\delta M} \end{aligned}$$

With these relations in mind, a graph of the expected force can be derived for a given local field intensity with which motion is resisted. A particle that is sufficiently cold to superconduct will thus see a valley that follows the magnetic equipotential lines; only when the perpendicular force is suffiently large will the valley be ignored.

Transport surfaces

If the powder is levitated, there will be no action that will encourage the clusters to break up. Indeed it is favorable for mildly magnetised powders to cluster, as this reduces their total surrounding space and hence the volume which their field oddity affects. It is disadvantageous to allow such clumps to lift off, as there is then no way to break them up. Some form of repeated levitation could be used as the clumps would be disturbed whenever they 'land'.

In general, then, the powder will have to move on some sort of surface. Brass, aluminium and glass were tried; these all appeared to get equally dirty but allowed the powder generally to move. Such dirt can not be allowed to accumulate on any apparatus that intends to slide the material, as it will be randomly affected by the stuck powder that preceded it. Plastics, on the whole, appeared to suffer equally, but when polished

clean appeared to resist such effects more readily. It was found after some experimentation that PTFE was able to carry the material and usually allow it to slide freely for no reason that has been ascertained at this time. On some occasions the powder would tend to dirty the surface, but not as much as had occured with the metals. A vigorous polish was used to generate surface charge (liquid nitrogen being an insulator), on a another occasion an electrostatically charged ramp was used to deliver powder onto the surface but neither of these appeared to make much difference to the behaviour of the material.

Linear methods

How should the force due to the magnetic interaction be applied ? A magnet may be passed underneath a surface covered with powder to push material ahead of it subject to the 'sticking' of the clumps to the surface. Temperature and/or field gradients can grade the powder by finding the limit before superconductivity fails as is shown in diagram 2.1.

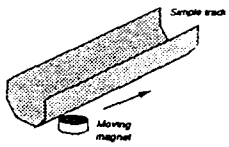

Diagram 1: Linear separation of a fine powder

Such a technique was tried; the results were similar to those found elsewhere[3]. The separation suffers due to the active region being the area immediately in front of the magnet, limiting the sample size for separation to the small amount of powder that can occupy that tiny region. If too much power is used separation will not occur as large amount of material that is not superconducting will be carried along by the remainder.

This is a useful technique but is limited to situations where fractions of a gramme sample size is not a liability. It is especially attractive to chemists who are searching for a minority phase with abnormally high T_c.

Area methods

It is possible to extend a linear separation method by widening the track and the moving magnet so that the separation region is wider, being the width of the track. Unfortunately, any imperfection in the track or the magnetic field will progressively tend to collect the powder into heaps which are swept along. If the track is not level, the powder tends to drift across the track in the downhill direction. It is these difficulties that make area methods impractical.

Vibration methods

Powder placed on a shallow incline may be moved 'downhill' by forcing the surface into a vertical mode of vibration. Such a slow vibrated transport can move powder past a grading station, normally a fork in the track, with one exit shielded by a magnet and the other by a small uphill slope. The powder moves past the station in a continuous stream, so that while the instantaneous active volume is unchanged, the total sample size can be much bigger.

An apparatus was constructed for this technique which operated successfully and was able to separate powders into two parts; one superconducting at the ambient temperature and the other not. During any run, however, the transport surface would cover itself with large amounts of powder and the smooth transport would fail making continuous operation impossible. The implementation is termed an overall failure, partly because the stuck powder cannot be reclaimed after removal and partly because the frequent cleaning required continuous operator attendance.

Dropping Methods

The methods described so far involve sliding the powder along a track. An alternative application of the magnetic force would be to levitate falling powder. Powder that is dropped onto a magnetic field will be repelled, allowing the unaffected powder to be discarded. A number of variants are possible, those that have been tested are described below.

If the powder is poured onto a simple magnet, the superconducting powder will fall next to the magnet due to the convex shape of the magnetic field. A magnet must be used with a hole in the middle in order that the magnetic field is slightly concave and the powder remains in a known position.

If the powder drop path passes through the area where levitating powder is collecting then later powder particles can knock levitated powder through. It is necessary to ensure that the levitated powder is to one side of the falling powder.

This method has not solved the problem with the powder remaining in clumps. It might be hoped that, if dropped from a sufficient height, that the forces involved in the deceleration might disrupt the clumps. The kinetic energy necessary for this to occur is well above the power of the levitation so that good superconducting material will not stop.

The magnet can be placed to one side of the drop path in order to deflect the falling powder away from itself. The pinning forces, being the main effector in this situation, are not concerned with the direction of the magnetic field gradient; the magnetic levitation force will primarily try to keep the powder at a constant magnetic field. Thus, as the powder passes the magnet, it will at some point be tangent to it. Thereafter the field will be decreasing and the powder will experience a net attractive force towards the magnet. The combination of initial repulsion and subsequent attraction make this method very difficult to implement and attempts at simplifying the situation failed. Results have been reported [3] suggesting that this method is possible.

If the powder never needs to leave the vicinity of the magnet, the unpredictable attraction described above will never occur. This can be set up if the magnet is a concave track that leads powder from its originally vertical path away from the vertical drop and into a container. Two magnetic arcs, as in diagram 2.2, can provide such a field. It was unfortunate that this method could not be tested as the magnets necessary would not have been ready in the time scale available. It is hoped that it can in future be tried.

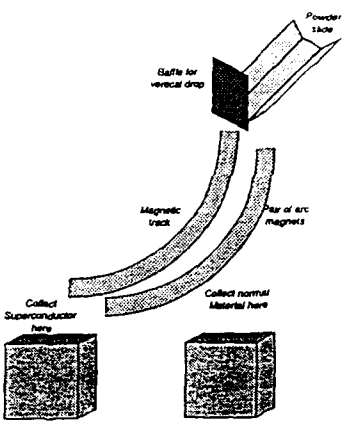

Diagram 1.2: Magnetic track separation method

Appendix II

Wet Separation

Internal Report by Dr.F.J.Blunt

Magnetic separation of superconductors

F.J. Blunt, A.M. Campbell

IRC in Superconductivity, West Cambridge Site, Madingley Road, Cambridge CB3 0HE

Abstract

In this paper two designs of magnetic separator are described. One is suitable for separating a small quantity of superconducting material from a large quantity of normal material. The other is particularly useful for the rapid separation of large quantities of superconducting material. Each uses a permanent magnet, runs immersed in liquid nitrogen and is very simple to build.

Keywords: High Tc, Magnetic separation

Introduction

Magnetic separation has been used industrially for the removal or separation of ferromagnetic materials for many years. Both the attraction of a magnet for a ferromagnetic material, and the repulsion between magnetised objects has been exploited. The separation of superconducting materials from non-superconducting materials can also be achieved magnetically, using the diamagnetic properties of superconductors. Levitation is widely demonstrated in these materials, and it is this property, combined with careful magnet design which is used to achieve separation. Magnetic separation has already been demonstrated using this principle (1), but the design only allowed a 'one off' separation of a very small quantity of material.

Magnetisation of Superconductors

Levitation of a particle lowered towards a magnet surface can be understood by analysing the magnetisation of the particles as they approach the magnet. The typical form of a magnetisation curve at 77K for a large grained sample of YBCO is shown in figure 1. When lowered towards a magnet the force experienced by the particles is given by the product of the magnetisation M and the field gradient. The magnetic field experienced by a particle descending along the axis of a cylindrical magnet close to one of its poles is shown in figure 2(a), and the resulting field gradient is shown in figure 2(b). Levitation occurs a few millimetres away from the surface. The overall field pattern is shown in figure 2(c). It is to be noted that particles falling near the outer edge of this magnet will be repelled away from the magnet altogether.

Magnetisation of superconducting particles is also a function of particle size and the reduced temperature, T/Tc. High Tc superconductors have rather large penetration depths - of the order of 0.4 micron in liquid nitrogen for YBCO. The magnetisation of particles as a function of the ratio of their radius to the *London penetration* depth has been calculated by Clem (2). Measurements carried out in this laboratory (3) support his calculations. The magnetisation of a 5 micron diameter particle of YBCO in liquid nitrogen is only about 30% of that of a large particle. This suggests that particles less than approximately five microns in diameter may levitate poorly. It has been observed by Solin (4) that very small particles of YBCO tend to be non levitating.

Magnet Geometry for separation of small quantities of superconductor

The magnet geometry of particular interest is a hollow cylindrical permanent magnet. This can be modeled as two counterwound coils, the inner coil representing the material missing from the centre.

Using the Biot-Savart Law the field at a point P on the axis, a distance z from the centre has a value given by the magnetisation of the material, and a geometric factor, which is given by

Field at P α cos θ_1 - cos θ_2 + cos θ_3 - cos θ_4
using the notation given in figure 3.

This magnet has an interesting field pattern. The field along the axis is illustrated in figure 4(a). The field calculated from the model corresponded very closely to the field measured in the laboratory. The field gradient is illustrated in figure 4(b), and the product M dH/dz is illustrated in figure 5. The values of M have been taken from the curve of M versus H measured experimentally for YBCO (figure 1). The points of stable levitation are marked on the diagram, where the force is equal to the gravitational force per unit volume on the particles. It is interesting to note that there is a second position of stable levitation beneath the magnet, for particles which have been pushed through the hole. We have succeeded in showing this phenomenon in the laboratory, and the distances between the particles and the magnet correspond closely to those calculated.

There are a number of important features to note in figure 5. First there is a minimum magnetisation required to ensure that the maximum force, marked point A on the diagram is sufficient to achieve levitation. Secondly levitation actually appears in this geometry while the particle is in the diamagnetic slope of its hysteresis curve. This is due to the fact that the field in this magnet passes through a minimum close to the magnet surface. The point A is reached when the particle reaches the maximum in its magnetisation curve. Thirdly the force rises very steeply, so the levitation is stable, and minor disturbances of the particles will not cause them to fall through. Unfortunately the force on the particles changes by a factor of about 3 within the space of approximately one millimetre. This means that separating particles of differing magnetisation will not be possible in this geometry.

An additional feature peculiar to this magnet geometry is that there is a centring force on the particles, which keeps them neatly placed over the hole. The field profile off the axis of this magnet is shown in figure 4(c).

This magnet geometry is ideal for the separation of a small quantity of superconductor from a large quantity of normal material. The design is shown in figure 6. The chief points in the design are as follows.

1) The particles are placed in a sieve at the top (approximately 30 micron aperture). This is vibrated so as to allow a fine rain of powder into the liquid nitrogen. This minimises particle clumping, which would result in poor separation of material.

2) The particles fall through a reasonable depth of liquid nitrogen before they reach a significant magnetic field. This is to ensure that they become magnetised. In practice it was found that 10mm was sufficient. Without taking this precaution the superconducting particles tend to fall straight through the hole.

3) A side arm is provided for removal of the superconducting material by suction. Particles removed from the central zone must be carried over the top surface of the magnet without being allowed to settle, since there is insufficient upward force on the particles in this region to keep them levitating. Once near the outer edge the magnetic field repels the particles away from the magnet. It was found that periodic suction achieved a very efficient removal of particles. Since the particles are carried in the refrigerant they do not come to rest in the tube. They fall into a container beneath the outer edge of the magnet.

Efficiency of separation.

This process achieves a very efficient separation, but because sieving must be halted frequently to clear the central area it is not suitable for large quantities of material. The aspect ratio and hole diameter of the magnet was studied in some detail. It was shown that the position of the maximum dH/dz was very insensitive to the magnet shape. The smaller the hole, the larger the maximum value of dH/dz was achieved. Therefore a reasonable choice of magnet for a separator would be approximately 30mm diameter, 10mm thick, with a hole 6 to 8mm diameter.

All material which levitates is superconducting, although obviously some non superconducting material may adhere to it. Using a sieve at the top prevents loose material adhering to the superconducting particles, but if the manufacturing process gives a multiphase material, it is clearly possible for second phases to remain adhering to the superconducting particles after grinding. A small amount of superconducting material will be lost, due to poor magnetisation. This loss can be minimised by careful control of the grinding process. Some particles will be lost if the material is allowed to collect in any quantity in the levitating zone, as descending non superconducting particles will knock the material through the magnet. This can be avoided by frequent clearing of this zone.

Magnet geometry for the separation of large quantities of superconducting material.

Experimentation led to the adoption of an alternative magnet geometry. The magnet has a conical pole piece and this has the field distribution shown in figure 7. The centring force is virtually absent, and particles falling toward this magnet tend to fall outwards. They do not fall onto the magnet surface, but instead remain levitated above the magnet surface. Preliminary experiments with this magnet resting on a white card showed that all the superconducting material fell outside a well defined ring, missing the outside edge of the magnet typically by two or three millimetres. No superconducting material was observed to fall in the inner region. The original design had a pole piece without a hole. This left a problem in removing the non superconducting material, which tended to collect on the pole pieces. When lumps of this broke away, they were sometimes able to find their way into the container reserved for superconductor. Experimentation showed that in this geometry it was also possible to use a magnet with a central hole, and in this instance the non superconducting material falls through the central hole. Containers can be placed strategically to collect the fractions. The finished design is illustrated in figure 8.

Efficiency of separation

This method is fast and continuous, which are the important prerequisites for an industrial process.

Conclusions

It is possible to construct a very simple magnetic separation system to achieve a high degree of separation of superconducting material from non superconducting material.

Aknowledgments

We would like to thank the European Office of Army Research for their support of this work.

References

1. Barsoum M. Patten D., Tyagi S, Appl. Phys. Lett. 51 1954 (1987)

2. Clem J.R., Kogan V.G., Proceedings of 18th Conferences on Low temperature Physics Kyoto 1987. Jap. J of Appl. Phys. 26 (1987) supplement 26-3, p.1161

3. Hibbs A.D., Eberhardt F.J., Campbell A.M., Male S., Cryogenics 28 678 (1988).

4. Solin S.A., Garcia N., Vieira S., Hortal M., Phys. Rev. Lett. 60 744 (1988).

Figure captions

1. A typical magnetisation curve for a large grained sample of YBCO measured at 77K.

2 (a) The magnetic field along the axis of a cylindrical magnet close to its pole.
(b) the field gradient, dH/dz of the magnet
(c) the field pattern in the pole region.

3. Modelling a hollow cylindrical magnet as two counterwound solenoids.

4.(a) the magnetic field along the axis of the hollow cylindrical magnet.
(b) the field gradient dH/dz of this magnet

(c) the field pattern in the pole region.

5. Force on a superconducting particle as it falls towards, and through, the hollow cylindrical magnet.

6. Design of a separator for removal of a small quantity of superconductor from a large volume of normal material.

7. The magnetic field profile close to the pole of the hollow conical magnet.

8. Design of a separator to separate large quantities of superconductor continuously.

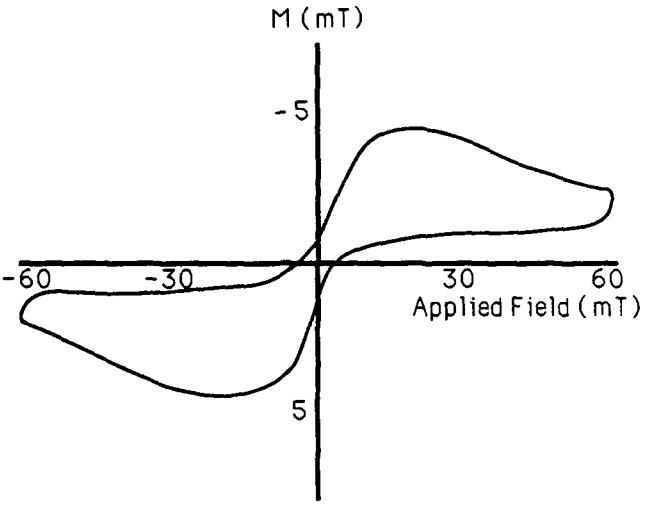

Figure 1: a typical magnetisation curve for a large grained sample of YBCO measured at 77K.

(a)

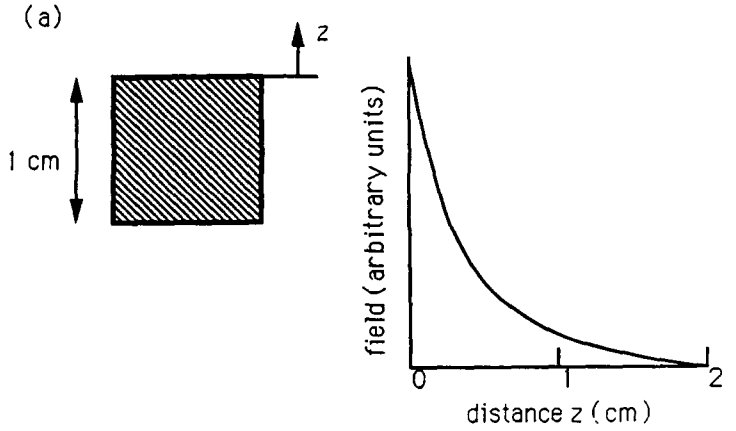

(b)

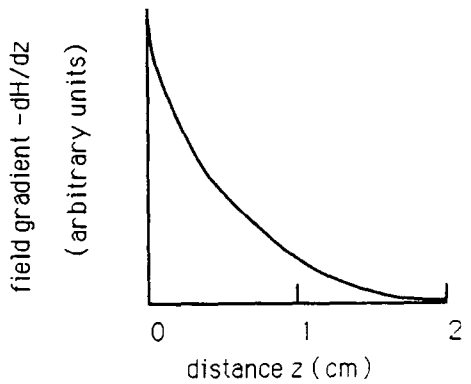

(c)

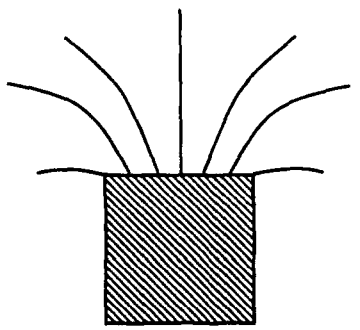

The magnetic field close to a cylindrical magnet

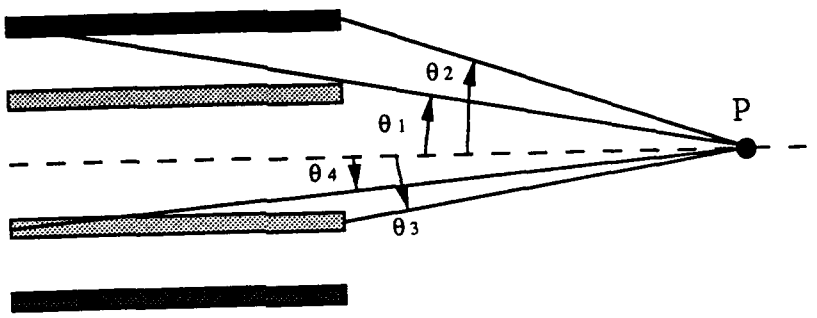
θ2
θ1
P
θ4
θ3

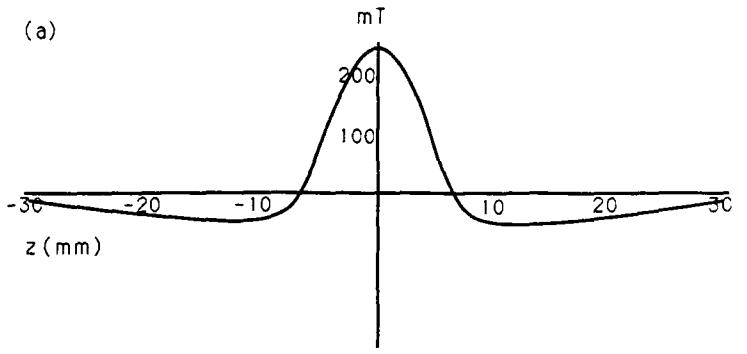

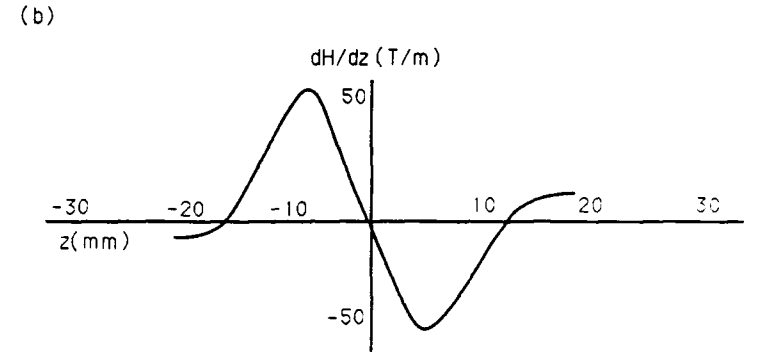

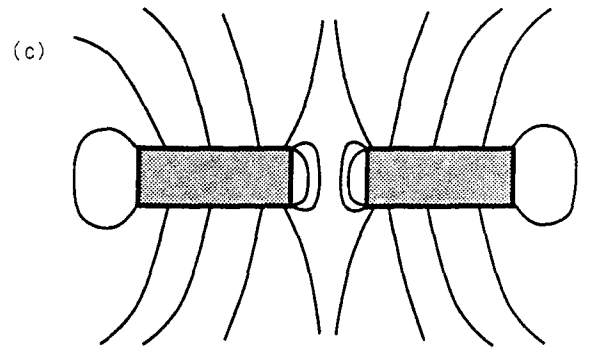

(a) Magnetic field for magnet available along its axis.
(b) field gradient of magnet along its axis
(c) field profile around the magnet

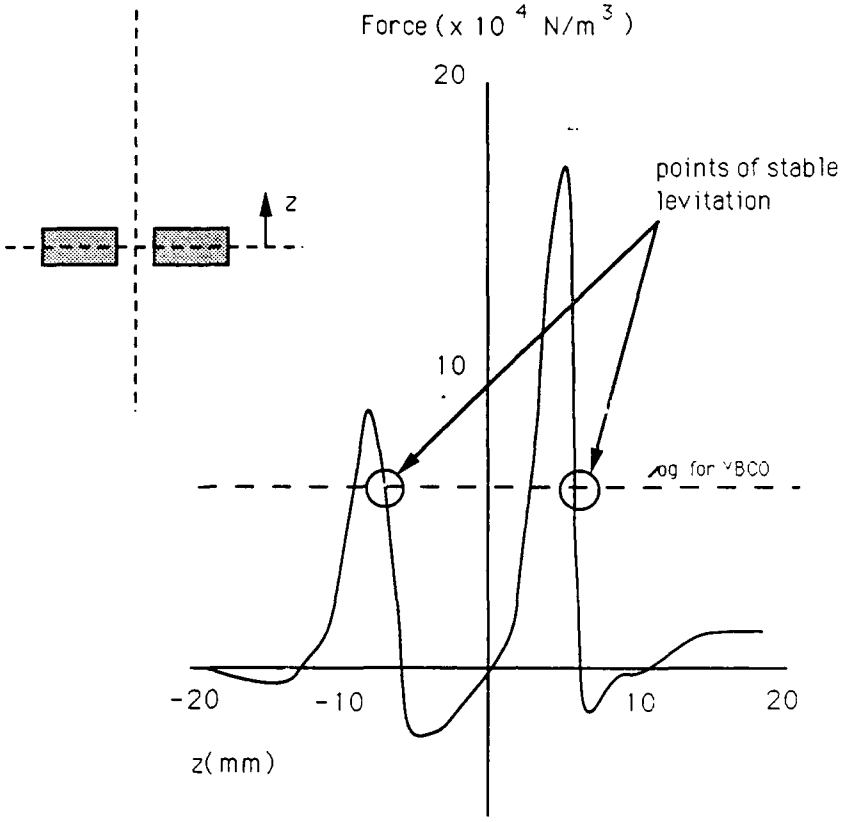

Force on a superconducting particle as it descends the z axis of the magnet.

Figure

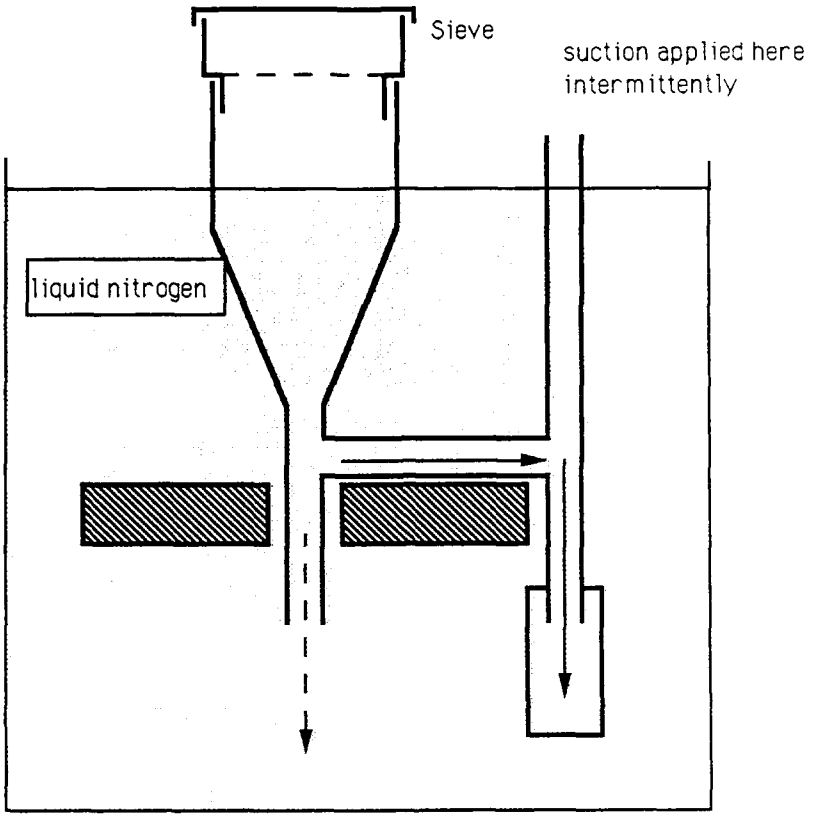

figure design of a separator for the removal of a small quantity of superconductor from a large quantity of normal material

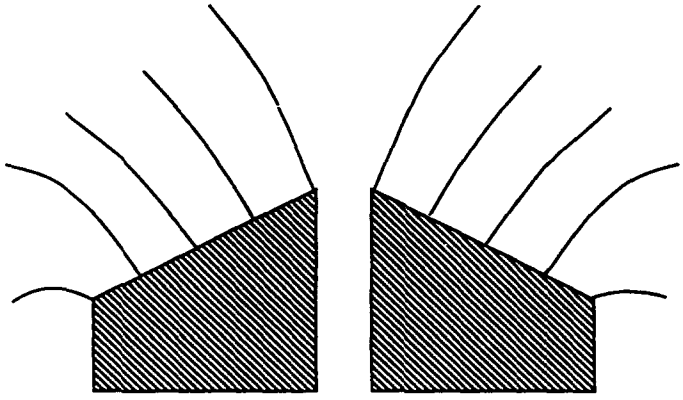

figure the magnetic field profile close to the pole of the hollow conical magnet.

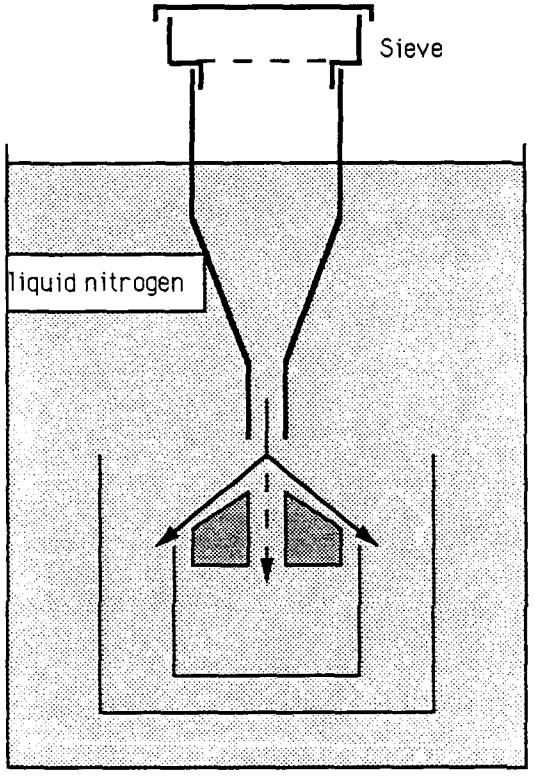

path taken by the superconducting particles

path taken by the non superconducting particles

length scale approximately 10 mm

figure . design of a separator for the rapid and continuous separation of large quantities of superconductor..

Appendix III

Levitation and Damping

Internal Report by A.Perry

1. Levitation

Magnetic bearings have been developed using superconducting coils to provide an opposing pair of magnetic poles that will raise rotating apparatus with little energy loss. A possible area of application of such bearings is in gyroscopes where very low rotational losses are required to provide a useful instrument.

A simple form of rotating levitation consists of spinning a *symmetrical magnet* about its axis above a superconductor sheet. A concave sheet is required to form a slight energy well that will stop the levitation moving around the levitating sheet and slightly later falling over the edge. The magnet, generally a short cylinder, has a magnetic field that is invariant under rotation about its axis. Since the magnetic flux between the magnet and the superconductor is not quantised, there will be no flux motion in the superconductor, no loss and hence no torque applied to it. In such a situation a gyroscope will run for long periods subject only to flux creep. Preliminary experiments showed that apparently symmetrical magnets suffer unusually large losses when rotated and levitated [1].

Magnitude of loss

If the levitated rotation sustains loss, the local field seen by superconducting particles must vary. The energy loss is the area enclosed by the cycling change in the magnetic state of the material. This area can easily be measured on a magnetisation curve as the physical situations are identical. The equations that relate a measured magnetisation curve to the critical current together with a discussion of one of the techniques of measuring the magnetisation using an AC magnetometer are described elsewhere [2] providing results similar to those in diagram 1.1 that were kindly provided by J. Blunt.

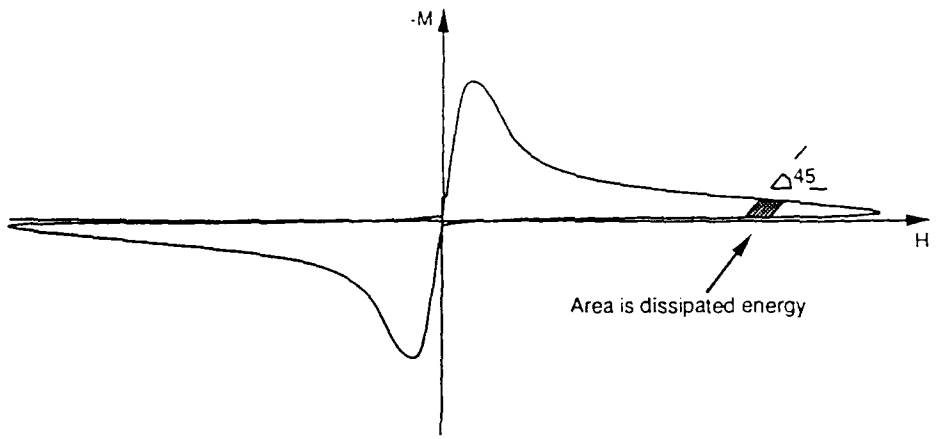

Diagram 1.2: Hysteretic loss on a magnetisation diagram

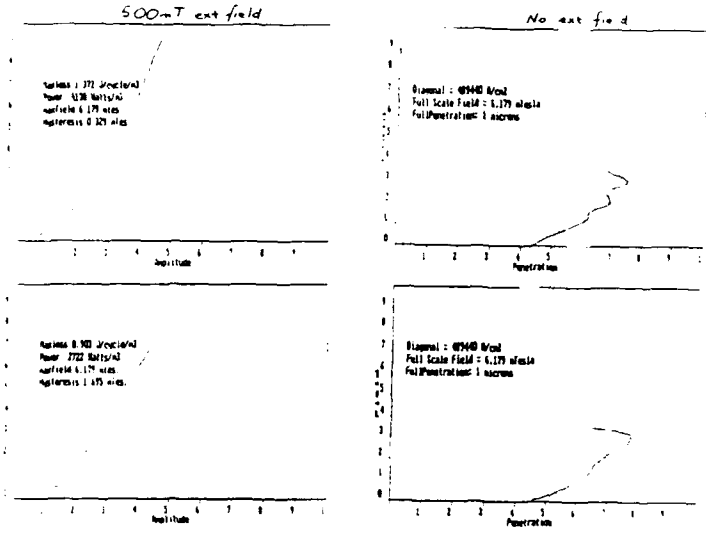

Diagram 1.1: Sample results for $Y\,Ba_2Cu_3O_{7-\delta}$, giving penetration depth, J_c, δM, δE

When the effective magnetisation of the material is not following the limiting envelope of the magnetisation curve, it tends to move with a gradient μ_0, leading to swept regions that are approximately parallelograms. If the external field varies between two limits H_1 and H_2, then the area enclosed for a small variation $\delta H = H_2 - H_1$ is $E = \delta M \times (\delta B - \delta M)/\mu_0$ and is conveniently linear in H when M is virtually independent of H. This is demonstrated in diagram 1.2.

For small field variations the changing field is screened by surface currents on the particles. An analysis of this state was made by London, who showed that the dissipated energy is approximately proportional to the cube of the field variation.

These two ranges can be combined into a single smooth curve as shown in diagram 1.3.

$$\delta E = \begin{cases} \frac{4}{27\delta M \mu_0}\delta B^3 & \text{if } \delta B < \frac{3}{2}\delta M \\ \delta M(\delta B - \delta M)/\mu_0 & \text{Otherwise} \end{cases}$$

The energy dissipated under levitation is constant for all points on the same circle about the axis of rotation. To calculate this dissipation for any such circle, we must consider the successive maxima and minima of the magnetic field along that circle.

$$\text{At } x = X_i, \quad \frac{dB}{dx} = 0 \text{ and } \frac{d^2B}{dx^2} \begin{cases} < 0 & \text{odd}(i) \quad [maxima] \\ > 0 & \text{even}(i) \quad [minima] \end{cases}$$

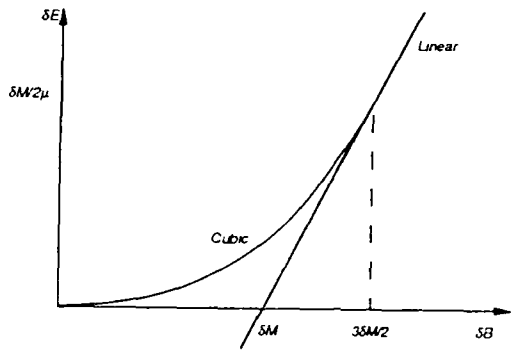

Diagram 1.3: Suggested energy dissipation with respect to field variation amplitude

hence

$$\frac{dB}{dx}\begin{cases} > 0 \text{ for} & X_{2i} < x < X_{2i+1} \\ < 0 & X_{2i-1} < x < X_{2i} \end{cases}$$

We must consider the energy dissipated for successive increasing and decreasing sections separately. To a useful approximation, we can use half of the dissipation calculated for a cycle between the two limits

$$\delta E_{here} = \sum_{i=1}^{n} \delta E \left(\left| B(X_i) - B(X_{i-1}) \right| \right) / 2$$

This dissipation will occur everywhere around the current circle, so we must integrate this through the entire superconductor sheet,

$$\delta E_{total} = \int_0^{z_0} \int_0^{\infty} 2\pi r \delta E_{here}(r, z)\, dr\, dz$$

For a thin sheet, the parameters can be taken as independent of the sheet thickness and the integral over z can be replaced.

$$\delta E_{total} = \int_0^{\infty} 2\pi r \delta E_{here}(r)\, dr$$

Deceleration

In the present discussion a cylinder rotating about its axis is considered, this will have a moment of inertia

$$I_{zz} = \frac{1}{2} M R^2 = \frac{\pi}{2} \rho z_0 R^4$$

Its rotational energy, E, reduces with time, decreasing by δE_{total} with each full rotation $\delta\theta = 2\pi$, thus

$$\frac{dE}{d\theta} = \frac{1}{2\pi}\delta E_{total}$$
$$E = \frac{1}{2}\omega^2 I_{zz}$$

Manipulation yields

$$\ln(\omega) = Constant - \frac{\delta E_{total}}{2\pi I_{zz}}$$

This result can be used to estimate the dissipation from measurements of the deceleration rates.

Loss of detail with distance

Consider a magnetic field in free space

$$\begin{aligned}\mathbf{B}(x,y,z) &= B_0\exp^{-z\omega}(\cos(\omega x),0,\sin(\omega x))\\ \operatorname{div}\mathbf{B} &= B_0\exp^{-z\omega}(-\omega\sin(\omega x) - \omega\sin(\omega x))\\ &= 0\\ \operatorname{curl}\mathbf{B} &= B_0\exp^{-z\omega}(0-0,\omega\cos(\omega x)-\omega\cos(\omega x),0-0)\\ &= 0\end{aligned}$$

A similar result applies for periodic effects in the y direction. Considering the $z = 0$ plane as the surface of the magnet, many surface profiles can be constructed using non periodic fourier algebra. The magnetic field in free space is linear and additive, so the results can be superimposed to find the expected field profiles at a distance from the surface. At a distance z from a periodic field component, the local magnitude of that component is reduced by a factor of $\exp(-z\omega)$.

Near the edge of a circular magnetic field, there is no first order and little second order variation tangential to the edge. This region can be modelled using a cut through the diameter, simplifying the algebra by using a function that is periodic every $4R$; where errors due to the virtual magnets one diameter away are significant. loss of resolution of the real magnet is sufficiently severe that the case need no longer be considered.

For a magnetic field circle of radius R, consider a periodic field function

$$\mathbf{B} = \begin{cases}(0,0,B) & (4n-1)R < x < (4n+1)R\\ 0 & (4n+1)R < x < (4n+3)R\end{cases}$$

Construct the usual sum of cosines together with a constant offset for this step. Since the surface of the circle is a constant magnetic field, there is no component of field in the x direction

$$\mathbf{B}|_{z=0} = \frac{B}{2} + \frac{B}{2}\sum_{i=1,3,5\ldots}\frac{(-1)^{(i-1)/2}}{i}\cos(i\omega x)\,(0,0,1)$$

The reduction factors for the fourier components can easily be inserted. This flattens the edge of the circle as can be seen in diagram 1.4. This result may conveniently be used in characterising the height of a measurement point from the magnetic circle by considering the maximum gradient of the field.

When $x = R$, differentiating $\mathbf{B}$ wrt x for a given height z yields

$$\begin{aligned}\frac{dB_z}{dx} &= \sum_{odd\ i}\frac{B\pi}{2R\sqrt{2}}\exp(i\omega z)\\ &= \frac{B\pi}{2R\sqrt{2}}\frac{\gamma}{1-\gamma^2} \qquad \text{where} \qquad \gamma = e^{\pi z/2R}\end{aligned}$$

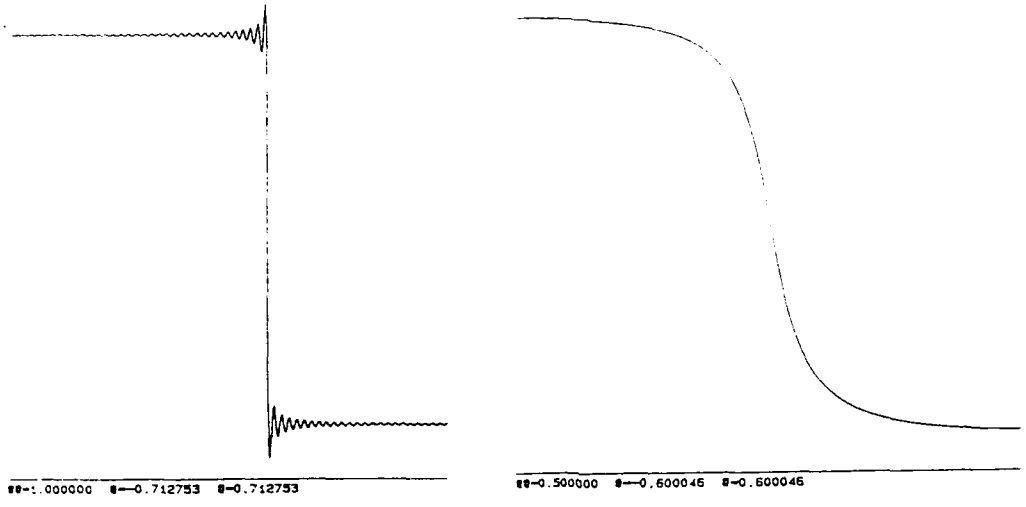

Diagram .4: Loss of definition when at a distance from a step in magnetic field

Small perturbations

Any local variation in the surface field of the magnet must be sufficiently large in area that it is visible from a distance, as the superconductor is likely to be at least 1 *mm* away. If a variation is to be effective then it must be visible on a scale of millimetres. The resolution of the field image must be finer than this by at least a factor of 5 in order to be able to map the shape.

If a very small variation occurs in the magnetic field covering large areas the feature will not disappear with distance and, over a large area, can cause large losses. In order to measure a gradual variation, a repeatable method is required so that the resulting signal has a lower noise level (after averaging) than the amplitude of such variations.

Inhomogeneities in the material used to form such a magnet and errors in its magnetisation can cause the magnetic centre and the centre of gravity to be separate.

$$\mathbf{c}_g = \int_V \mathbf{r} p \, dV$$

$$\mathbf{c}_m = \int_S \mathbf{r}\mathbf{B}.\,\mathbf{dS}$$

$$d_{gm} = |\mathbf{c}_g - \mathbf{c}_m|$$

At low rotational speeds, the magnet can rotate about its magnetic centre. There will be no loss accrued in the superconductor as the field is stationary and the moving centre of gravity merely requires the local levitating force to vary. The magnet will tilt very slightly down in the direction of the centre of mass from the magnetic centre. A very small field increase with negligible flux motion can provide extra lift (because

the local field is increasing) and the tiny field reduction on the other side can produce a relatively large reduction in lift.

$$B'(r) = B(r) + rB(0) \times Const$$

$$\delta B(r) = B'(r) - B(r) = B(0)\frac{rd_{gm}}{R^2}$$

While at low speeds the losses are negligible, at higher rotation speeds the centripetal force on the off axis centre of gravity can no longer be countered by the superconductor and the magnet starts to rotate about its centre of gravity. The magnetic field moves in circles; at each point the magnetic field changes apparent radius by twice the distance between the two centres. Thus

$$\delta B(r) = B(r)\,2d_{gm}\,\frac{dB(r)}{dr}$$

This is clearly much larger than the low speed loss.

If the edge of the magnet is chipped the field that would have appeared perpendicular to the face of the magnet will appear perpendicular to the surface of the chip. As can be seen in diagram 1.5, each chip will modify the local edge field, providing a surface field

$$\delta B(r) = B(0)(1 - \sin\theta) \quad \text{for} \quad R - w < r < R$$

This field step will be rounded by distance.

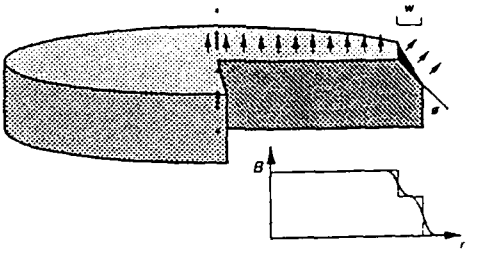

Diagram 1.5: Small field change due to a chipped magnet edge

Velocity measurement

In order to characterise the losses and vibration modes of a magnet undergoing levitation, a stopwatch suited to timing repeating events was needed. A simple stopwatch could not measure the change of frequency with time and so was not suitable to measuring deceleration.

There was no timer capable of the task conveniently available, so an additional subroutine to read data into the computer program **EXAMINE** (described in the next chapter) was created. This simple routine measures elapsed time between successive impulses and records the sequence of values into a data block

Inaccuracies in the measurement of absolute time for the instants (that are only accurate to $50\,ms$) can be reduced to insignificance by averaging or fitting the results to a curve.

An error in determining the position in time of an impulse affects the measured values of the neighbouring intervals in opposite directions. Averaging and curve fitting both reject such components very well.

Such preprocessing can be performed using the standard facilities of **EXAMINE**. The individual time intervals can be inverted into angular velocities and analysed to find required values.

It had been intended to use an optosensor that could be read directly by the computer to provide the signals. Difficulties were experienced due to frost deposition on the windows, due to the low temperature affecting the sensor and due to the difficulties in targeting the sensor unit on the correct magnet region. The most reliable method of acquiring impulses was using the human eye and brain for preprocessing and the keyboard for data entry. The repetetive nature of the signals made this easy and reliable.

Estimating feature sizes

It is well known that, for a given magnet and superconductor, there is a range of stable levitation heights available. These can be exploited when attempting to gain information about the magnetic field of the magnet. We have seen that, in order to be effective, features have to be at least as large as the levitation height; in fact, they must be comparable in size to the levitation height as the limited surface area of the magnet places an upper limit on the size of features that can occur.

We have already found how to determine the energy loss per rotation from a sequence of angular velocity measurements. If the resulting loss value is plotted against levitation height, classes of features may be recognised by their characteristic dimension.

A feature, on the verge of effectiveness, might have a dimension l characteristic of its size. The magnitude δB of the feature will be reduced according to the levitation height z and for $\delta B < \delta M$ the energy loss varies as δB^3. Then

$$\begin{aligned}
\delta B_i &= \delta B_o \exp -z/l_i \\
\delta E &= const \times \delta B^3 \\
&\propto exp(-3z/l_i) \\
\delta E &= \sum_i K_i \exp \frac{-3z}{l_i} \\
&= \sum_i K_i (\ln z)^{-3/l_i}
\end{aligned}$$

A plot of δE_{total} against $\ln z$ as in diagram 1.6 may allow estimates of feature sizes to be made. The results of this estimation for the magnet are given in the results chapter.

Magnetic centre displacement

An alternative to the rotation of the magnet about a vertical axis is to rotate it about a horizontal axis in the manner of a wheel. The description of the effects of a displaced magnetic centre as above still apply with the addition at very low speeds of a new effect.

At low speeds, the transverse force across the magnet due to gravity acting at the centre of mass can supply sufficient torque to stop rotation from occurring. The magnet then performs Simple Harmonic Motion

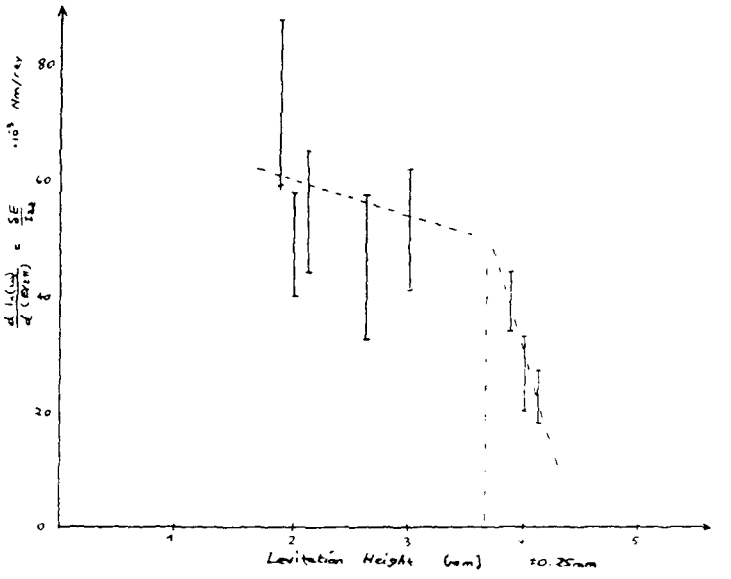

Diagram 2.6: Variation of loss with levitation height

about the position with the centre of gravity lowest. A measurement of the oscillation frequency ω of this motion for small amplitudes can provide an estimate of d_{gm}

$$\text{Torque} = T = d_{gm} M g \sin\theta$$
$$\text{Inertia} \approx I_{zz} = MR^2/2$$
$$\text{Off axis c.of.g.} \rightarrow \delta I_{zz} = M d_{gm}^2$$
$$\text{hence} \quad \ddot{\theta} = -\omega^2 \theta$$
$$\omega \rightarrow \sqrt{\frac{g\, d_{gm}}{d_{gm}^2 + R^2/2}} \text{ as } \theta_{max} \rightarrow 0$$

Magnetic Field Inhomogeneity.

To check the correlation between damping and superconductor loss it was necessary to know the field fluctuations induced by the magnet. The magnetic field was measured on a fine scale by rotating the magnet in a lathe close to a very small search coil (200 turns with an effective radius of 0.14 mm). The waveform was picked on a signal capture system and averaged to reduce noise. The main errors with this system arise from vibration in the lathe head which give synchronous voltages even with a perfectly homogeneous magnet. It was possible to eliminate most of these by tracking the coil across the magnet in different planes and looking for features associated with the magnet position rather than the lathe head position. It was also necessary to keep the coil very close to the magnet and then predict the field fluctuations at the larger distance of the levitated magnet. A contour map of the field fluctuations across the magnet surface follows (Fig.1). The surface field was 33 mT and typical field fluctuations about 3 mT. The largest component was caused by a small chip in the edge of the magnet.

Comparison with Damping

The loss per cycle for large speeds was increased because inertial forces caused the magnet to wobble. At low speeds the hysteresis loss was 3.5 nJ per revolution. The loss predicted from the field fluctuations was about five times larger than this which is acceptable agreement given the difficulty in measuring small field fluctuations on a fine scale. It appears that the superconductor hysteresis loss is sufficient to explain the damping observed. The very high value compared with Niobium is due partly to the low value of Hc1 in these materials and partly to their granular nature which means that there are losses on the surface of every grain . If high critical current densities could be carried across the grains the performance would be greatly improved.

6. References

[1] ONNES H.K. **Leiden Comm** Univ Leiden 122b 124c, 1911, Suppl 35, 1913

[2] BARDEEN J., COOPER LN., SCHRIEFFER J.R. Phys Rev 108, 1175, 1957

[3] LONDON F., LONDON H. Proc Roy Soc (London) A149, 71, 1935

[4] MEISSNER W , OCHSENFELD R. Naturwissenschaften 21,787,1933

[5] LAURMAN E., SHOENBERG D. Proc Roy Soc (London) A198, 560, 1949

[6] PIPPARD A.B. Proc Roy Soc (London) A216, 547, 1953

[7] GINZBURG V.L., LANDAU L.D. Zh.eksp.teor.Fiz. 20, 1064, 1950

[8] GORKOV L.P. Zh. Experim.i.Teor.Fiz., 1981, 36, 1959

[9] GORKOV L.P. Soviet Phys JETP, 593 and 998, 10, 1960

[10] LONDON F. "Superfluids" vol 1 Wiley NY, P152, 1950

[11] LABUSCH R. Crystal Lattice Defects 1,1,1969

[12] KRAMER E.J. J Appl Phys 44,1360,1973

[13] ESSMAN U., TRÄUBLE R. Phys Letter A26.526,1967

[14] ULLMAIER H. **Irreversible properties of Type *II* superconducters** Springer-Verlag 1975

[15] CAMPBELL A.M., EVETTS J.E. J Adv Physics, 199,21,1972

[16] BLUNT J. Pers. Comm. 1988

[17] CAMPBELL A.M., HIBBS A.D., EBERHARDT J., MALE S., ASHBY M.F., EVETTS J.E. **Magnetisation and Critical Currents in High T_c Powders**

[18] HAYASHI K., YOKOTA Y., *et al* **Separation and Characterisation of superconducting YBa2CuO7 Powder** Jap J Appl Phys, P1856, 10, 1988

Fig 1

Appendix IV

Magnetic Measurements on Hollow Cylinders

Paper in Cryogenics

Flux trapping and magnetization of hollow superconducting cylinders*

F.J. Eberhardt, A.D. Hibbs and A.M. Campbell

Interdisciplinary Research Centre in Superconductivity, West Cambridge Site, Madingley Road, Cambridge, UK

The magnetization of hollow cylinders of high T_c material and the field trapped inside them has been measured by integrating the signal from coils outside and inside the cylinders. The two coils allow the field trapped in the grains themselves to be separated from the field due to the circulating currents. The trapped field tells us the maximum field that can be expected in a magnet. If J_c drops rapidly with field the parameter which will determine the trapped field is not the zero field critical current density but the field at which it is reduced by half. A comparison is made of various preparation methods.

Keywords: high T_c superconductivity; magnetization; critical currents

Powders of yttrium barium copper oxide which have been compressed and sintered into a solid block show two superconducting pathways. One is confined to the individual grains (the intragrain current) and has a critical current density, J_c, of approximately 10^6 A cm^{-2} at 4 K[1]. The other can cross grain boundaries (the intergrain current), but has a much lower J_c in the materials fabricated so far. This is illustrated in *Figure 1*. For practical purposes it is necessary to bring the intergrain current density up to the values achieved within grains. When the material is exposed to a magnetic field the currents in the grains cause a magnetization of the material, and the intergrain currents form a screening current. This is illustrated in *Figure 2*.

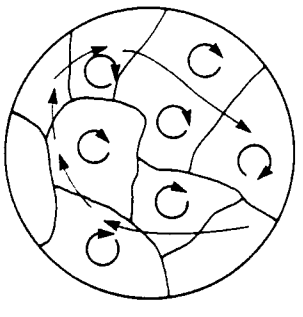

Figure 1 Alternative current paths in yttrium barium copper oxide: large currents within grains, small currents between them

*Paper presented at Critical Currents in High T_c Superconductors, Birmingham, UK, 16 May 1988

0011 2275/88/100681 04 $03 00

A hollow cylinder fabricated out of this material is an interesting geometry for a number of reasons:

1. it is possible to separate out the effects of the two currents, since the fields due to the flux in the core and the flux in the material are in the opposite sense in the core but in the same sense outside the cylinder, as shown in *Figure 2*;
2. this geometry may be used for screening purposes; and
3. it is easy to make and it may be the most effective geometry for making permanent magnets since it is a more efficient use of material.

Maximum screened field

The critical current densities of these materials fall very rapidly in the presence of a small magnetic field[2]. The fall is approximately exponential: illustrated schematically in *Figure 3*. If a field of strength B_i is required in the core of a solenoid of this material the wire would be restricted to operate at the critical current density J_{ci}. Since the current density in a solenoid is uniform the field will fall off linearly in the wall of the solenoid.

In contrast a magnet made from a solid block of this material would have a field profile which was not linear. The critical current density in the material would start at J_{ci} in the centre and rise as the ambient field fell, reaching the zero field value of J_c at the outer edge. Hence, the thickness of material required would be less. It is worth pointing out that if the fall of J_c with applied field is approximately exponential an important parameter for these materials will be the value of field at which the critical current density has fallen to half the zero field value, as from this point the size of cylinder required to contain a larger field will rise exponentially also.

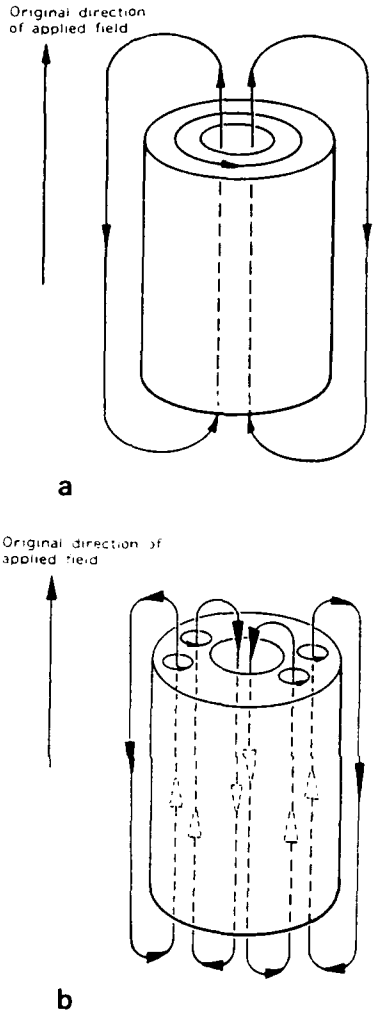

Figure 2 Schematic diagrams showing: (a) circulating bulk currents trapping flux in the core, (b) currents in grains magnetizing the material

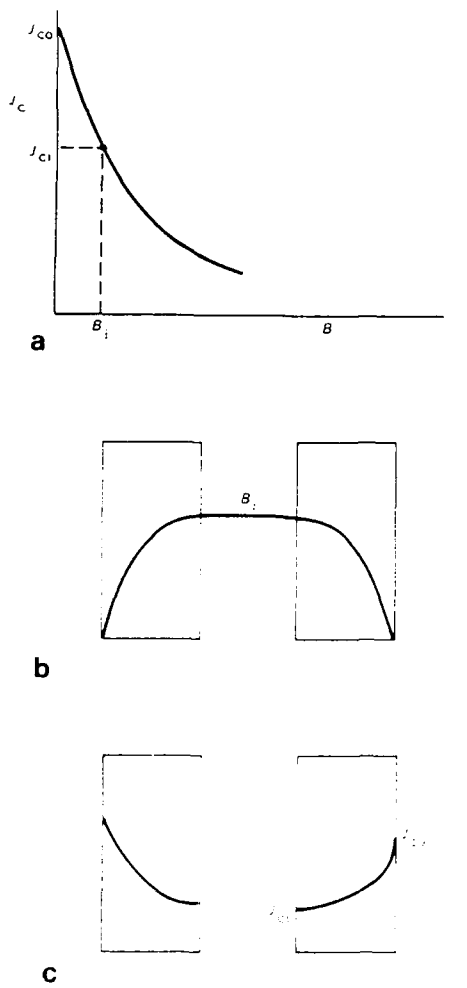

Figure 3 (a) Fall in critical current density J_c with field (b) Profile of B in solid cylinder wall when a field B_i is trapped in the centre (c) Profile of J_c in solid cylinder wall when a field B_i is trapped in the centre

This follows from the critical state equation. If this field is denoted B_a the critical state equation is

$$\frac{dB}{dx} = \mu_o J_{co} \exp(-B/B_a)$$

where J_{co} is the zero field critical current density. This has a solution

$$\mu_o J_{co} d = B_a[\exp(B_i/B_a) - 1]$$

It can be seen that when $B_i > B_a$ the wall thickness rises exponentially.

If the material was fabricated into wire the thickness of solenoid required to hold back the same field would be

$$\mu_o J_{co} d = B_i \exp(B_i/B_a)$$

The thickness of wall predicted from this equation is always larger than for the case where a solid block of material is used, since in the latter case the full potential of the material to carry currents between J_{ci} and J_{co} is being used.

In this work cylinders of sintered YBCO have been fabricated. Magnetic fields have been applied to these, and the fields inside and outside have been measured using coils.

Experimental procedure

Yttrium barium copper oxide was made by mixing yttrium oxide, copper II oxide and either barium carbonate or

barium nitrate in the correct stoichiometric proportions and firing at 950 C for several hours. The powders were ground and pressed into moulds to give cylinders of the approximate dimensions 8 mm i.d., 14 mm o.d. and 10–13 mm long. Some powders were pressed dry and some were wet with acetone to facilitate handling. All cylinders were annealed in flowing oxygen. Two further cylinders were fabricated from bismuth calcium strontium copper oxide to the stoichiometry (1 : 1 : 1 : 2).

The cylinders were cooled in liquid nitrogen and exposed to a magnetic field for about half a minute. Two coils were wound, each with 800 turns, one to fit into the core of the cylinder and the other to go outside it (see *Figure 4*). The superconducting cylinder was lowered into the larger coil or passed over the smaller, inducing voltages which were integrated. The coils themselves were rather sensitive to movements in the earth's field and so were kept stationary.

The magnetization of the bulk material can be modelled by considering it to be equivalent to two opposing current sheets on the inner and outer surfaces of the cylinder. (It is assumed that the magnetization of each grain is the same). The signal in a search coil is then given by

$$\int V\,dt = M(L_i - L_o)$$

where M is the magnetization of the sample, and L_i and L_o are the mutual inductances between the search coil and close wound one turn per metre coils on the inner and outer surface of the cylinder, respectively. By a one turn per metre coil we mean the inductance of a closely wound coil of n turns per metre divided by n.

Intergrain currents flowing in a shell of thickness w give a signal

$$\int V\,dt = J_c w L_m$$

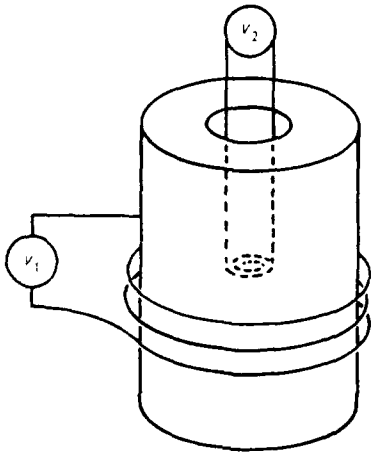

Figure 4 Schematic diagram showing the arrangement of the measuring coils

where J_c is the critical current density of the intergrain current and L_m is the mutual inductance between the search coil and a one turn per metre close wound coil filling the layer of thickness w.

In the extreme case of an infinite cylinder the inner coil responds only to J_c and the outer coil to the sum of the currents. In finite sized coils the coupling is still different but to extract the values of J_c and M separately it is necessary to calculate the mutual inductances

Mutual inductances were calculated using the formulae and tables in Reference 3. These formulae are for single layer coils. A computer program was written which treated each coil as a succession of concentric slices. Each slice was treated as a single layer coil of the appropriate mean radius and winding density, and the contributions from each layer in one coil to each layer in the other summed. The calculations were checked by measuring the signal in a third coil, and the agreement between calculated and measured signals was within 7%.

Results

In almost all samples the field in the centre coil was in the same sense as the applied field, indicating the presence of trapped flux. When a cylinder was slit axially, the bulk current pathway was interrupted and the signal changed sign.

It was originally assumed that since the critical current density falls so rapidly with applied field, almost all of it could be considered to be flowing in a region approximately 1/5th of the cylinder wall thickness around the outside edge of the superconducting cylinder. This assumption was checked using cylinders in which the signal had been measured both on a complete cylinder and one which had been slit axially. This revealed that the two coils gave comparable values for J_c if the currents were considered to flow in the region close to the centre surface of the cylinder wall. We believe that this is due to the fact that in these samples the magnetization and trapped flux produce fields of similar magnitude in the centre, causing the net field experienced by the material to be lower on the inner surface than the outer surface.

The results are shown in *Table 1*. Samples 1–3 were all made using barium carbonate as precursor. It can be seen that there is very little difference between those fabricated with the aid of acetone and those which were not. The handling of wet powder was much easier than dry powder. Critical current densities are low. However, these are not zero field critical current densities. There is a field of up to 3 mT trapped in the core, as the cylinder walls are quite thick. The best sample used barium nitrate as one of the precursor materials (sample 4). This had a critical current density five times better. Two cylinders were also made from the bismuth calcium strontium copper oxide material (1 : 1 : 1 : 2). One was ground to a powder and its diamagnetic susceptibility measured. This showed that the material contained both the high T_c phase ($\approx$110 K) and the lower T_c phase ($\approx$85 K), and the overall susceptibility was comparable to the material used in samples 1–3. The second cylinder was tested for trapped flux. No signal was detectable from the centre coil and the outer coil gave a very small signal. This enables us to put an upper limit on M of 0.1 mT but we cannot say whether there are significant intergrain

Table 1 Results of critical current density and magnetization measurements on samples 1–5

Sample number	Method of manufacture	J_c (A cm^{-2})	Magnetization (mT)
1	Powder pressed dry	77	0.72
2	Powder pressed wet	66	0.18
3	Powder pressed wet	72	0.53
4	Powder pressed dry (nitrate precursor)	370	1.7
5	Bismuth compound	?	?0.1

currents present. These results are consistent with magnetization results[4].

Conclusions

The measuring technique developed can give values of intergrain currents and magnetization without requiring contact to be made to the specimen. Like all measurements without a bias field there are considerable uncertainties, as the magnetization is not itself constant in the presence of small fields. The geometry described is suitable for the manufacture of permanent magnets once critical current densities are raised to a more acceptable level. Although the bismuth compound is easier and cheaper to make than the yttrium compound, preliminary results suggest that it has exceedingly small critical current densities.

Acknowledgement

The authors would like to thank the US army for their support of this project.

References

1 **Campbell, A.M., Hibbs, A.D., Eberhardt, J., Male, S., Ashby, M.F. and Evetts, J.E.** Magnetization and critical currents in high T_c powders. Paper presented to the Conference on High T_c Superconductivity, Boston, USA (1987)

2 **Kupfer, H., Apfelstadt, I., Schauer, W., Flukiger, R., Meier-Hirmer, R. and Wuhl, H.** *Z. Phys. B* (1987) **69** 159

3 **Grover, F.W.** *Inductance Calculations* Dover Publications Inc., USA (1973)

4 **Hibbs, A.D.** Personal communication (1988)

Appendix V

Theory of Screening

Paper in Superconductor Science and Technology

Supercond. Sci. Technol. 1 (1988) 65–67. Printed in the UK

Screening by high-T_c superconductors

A M Campbell
Interdisciplinary Centre for Superconductivity, West Cambridge Site, Cambridge, UK

Received 26 May 1988

Abstract. An analysis is made of the screening of low-frequency magnetic fields by high-T_c superconductors. Screening can occur either through the cumulative effect of a composite of isolated diamagnetic particles, or by the induction of bulk transport currents if the particles are connected. In the former case it is possible to define a screening parameter $s = t/\mu a$ where t is the screen thickness, μ the permeability and a the size of the system. There is only significant screening if the parameter is large. Even when screening is significant demagnetising effects put a rather low limit on the maximum field that can be screened so the conclusion is that screens made up of insulated superconducting particles are likely to be of very limited application.

1. Introduction

The diamagnetism of high-T_c superconductors is divisible into two components. One is due to currents passing between grains, the other to currents within grains. Since it is proving very difficult to carry high currents between grains it is of interest to determine how useful an array of independent diamagnetic grains might be for the purposes of screening and levitation. Screening due to transport currents must be treated separately.

2. Fields in composite superconductors

It is first necessary to establish the extent to which the classical theory of permeable materials can be used. A reversible type II superconductor of any shape can be treated as an ordinary magnetic material provided we define H for any value of B as the external field in equilibrium with that B in a long cylinder parallel to the field [1, 2]. The magnetisation, M, is then defined in the general case as $B/\mu_0 - H$. If we make a composite consisting of isolated particles of this material we can still use the same expressions and definitions. We define B as the average flux density over a region large compared with the particle spacing and obtain the B–H curve by measuring the flux density in a sample of zero demagnetising factor.

If, as is normally the case, the magnetisation is dominated by hysteretic effects the theoretical arguments based on thermodynamic equilibrium break down, but the magnetic behaviour does not depend on the assumptions of equilibrium provided the field is changed monotonically. The behaviour of a material consisting of insulated particles depends only on local values of B and the $H(B)$ curve, as measured on a long thin sample, if we now define H as the external field in this experiment. We can then imagine a reversible material with any $H(B)$ curve we like and choose one identical to the increasing (or, if appropriate, decreasing) curve of the irreversible superconductor. The irreversible material will behave in the same way as the imaginary reversible material provided there are no regions in which the local currents reverse, and provided we do not try to use expressions involving the entropy of the system.

To make the problem tractable we can split the magnetisation curve into three regimes. At low fields the material is linear and reversible with a small permeability. This holds up to a value of H where the magnetisation goes through a maximum. We shall call this H_m. At higher fields the material can be regarded as a permanent magnet with a magnetisation determined by the applied field. This magnetisation is small compared with H and will be positive or negative according to whether the external field has been increased or decreased. It does not change rapidly with field.

3. The permeability of composites

The permeability of a composite is not easily calculated in the most general case. For a dilute array we can add up the moments of individual particles in the applied field and extend the range of validity by using the Lorentz theory of dielectric constants. The result for a volume fraction f of spherical particles is $\mu = 1 - 3f/(f + 2)$.

A concentrated array is more likely to be of practical interest and we can calculate the permeability of a set of superconducting cubes with a thin air space between them, provided we apply the field perpendicular to the cube faces. If the gap between each cube face is $2d$ and the cubes have side a, the permeability is just the area fraction of free space on a cross section, i.e. $\mu = 4da/a^2$. The volume fraction is given by $1 - f = 6da^2/a^3$ so $\mu = \frac{2}{3}(1 - f)$. More complex geometries are best worked out by using the analogue of an array of

0953-2048/88/020065 + 03 $02.50

electrical conductors in place of the interstices between the grains, but the effect will only be to change the $\frac{2}{3}$ into another similar factor. It should be remembered when working out the effective volume fraction at high densities that even if the grains are touching there is an effective air space equal to twice the penetration depth between the grains.

4. Screening

We assume the material is linear with a permeability μ.

4.1. Case (i). A spherical shell of superconductor in a uniform external field H_0

This can be solved exactly by using a magnetostatic potential containing dipole and uniform field terms and matching boundary conditions at the inner and outer radii. If the external radius is a, and the internal radius is b, then the interior has a uniform field H_i given by

$$\frac{H_0}{H_i} = 1 + \frac{2}{9\mu}\left(1 - \frac{b^3}{a^3}\right)(\mu - 1)^2.$$

If we put $t = a - b$, and assume both small μ and small t/a this expression reduces to

$$H_0/H_i = 1 + 2t/3\mu a.$$

In order to get significant screening we must have $\mu \ll t/a$. To take a specific example if the thickness is 10% of the external diameter and $\mu = 0.01$ the field is reduced by a factor of 8. It can be seen that the material must be very close to complete densification if reasonable screening factors are to be obtained. Since there is inevitable penetration of each particle by λ, as well as the distance occupied by currents in the grains, it is also important not to use very small sized particles.

We shall define the screening factor s by $s = t/\mu a$, i.e. the relative thickness of the screen divided by the mean permeability. A similar parameter can be defined for most geometries. In this case if s is large the field is reduced by a factor $2s/3$.

The maximum field that can be screened is considerably smaller than the peak of the magnetisation curve. If t/a and μ are both small the maximum value of the effective H in the material is $H_0(\mu + 2t/3a)^{-1}$. For small s the internal field is increased by a factor $1/\mu$ and for large s it is increased by a factor $1.5a/t$. For the example given above it is $15H_0$. Hence the maximum field that can be screened is about $H_m/15$ or typically 1 mT. This can be understood from the fact that the energy available to exclude the field depends on the volume of superconductor, so thin shells cannot exclude such large fields as solid spheres. Results for cylinders are qualitatively similar to those for spheres.

4.2. Case (ii). Magnet inside a diamagnetic shell

This can also be solved in a similar way, and the results are similar to those of § 4.1. The ratio of the dipole moment without screening to that measured outside the screen is

$$1 + \frac{2}{9\mu}(\mu - 1)^2\left(1 - \frac{b^3}{a^3}\right).$$

This is the same as the screening factor for the uniform external field. The factor by which H is increased in the material is also the same as in § 4.1.

4.3. Case (iii). Infinite sheet

If the magnet is placed close to an infinite flat sheet, we can find the field on the other side of the sheet. There are a number of different configurations, but the basic problem is the same as that of a point charge above a dielectric sheet. To obtain the results for the magnetic case it is only necessary to replace E by H and ε by μ. The solution can be found in Smythe [3]. If we put a charge q at the origin, and a sheet of thickness t and dielectric constant ε perpendicular to the z axis, the field on the other side of the sheet is

$$\frac{q(1 - \beta^2)}{4\pi\varepsilon_0}\int_0^\infty \frac{kJ_0(k\rho)\,e^{-kz}}{1 - \beta^2\,e^{-2kt}}\,dk$$

where $\beta = (\varepsilon - 1)/(\varepsilon + 1)$ and ρ is the radial distance from the z axis. This can be written as the sum of the fields due to a set of image charges by expanding the bottom line with the binomial theorem. The potential is

$$\frac{q(1 - \beta^2)}{4\pi\varepsilon_0}\left(\frac{1}{(z^2 + \rho^2)^{1/2}} + \frac{\beta^2}{[(z + 2t)^2 + \rho^2]^{1/2}} + \frac{\beta^4}{[(z + 4t)^2 + \rho^2]^{1/2}} \cdots\right). \quad (1)$$

Notice that this does not depend on the position of the screening sheet. Only the distance to the charge, z, is relevant. This expression can be applied directly to a magnet with widely separated poles, each of which behaves like a point charge, but similar results will be obtained for other shapes. The image system, which is always valid, consists of a charge reduced by $(1 - \beta^2)$ in the original position, with charges $\beta^2(1 - \beta^2)$ at $z + 2t$, $\beta^4(1 - \beta^2)$ at $z + 4t$ etc. This applies to all magnets and coils. The maximum screening is with the magnet touching the screen and the test point immediately on the other side of the screen. Then $z = t$ and $\rho = 0$ and if $\beta \simeq 1$ the series can be summed. We find that the field on the axis is reduced by a factor of 4.9μ. If $z \gg t$ the exponential on the bottom line can be approximated to $(1 - 2kt)$ and the integral becomes

$$\frac{q}{4\pi\varepsilon_0 z^2}\int_0^\infty \frac{x\,e^{-x}\,dx}{1 + sx/2}$$

where $s = (\varepsilon - 1)^2 t/\varepsilon z$. The screening factor for this geometry, using superconductors, is $s = (\mu - 1)^2 t/\mu z$.

It can be seen that for small μ the value of the integral depends on $t/\mu z$. This is a similar factor to the one appearing in the screening by complete shells, with the distance to the magnet replacing the shell radius. For small values of s the field is reduced by a factor $(1 - s)$. Numerical integration shows that in general the field is reduced by about 0.6 when $s \simeq 1$ and the minimum is

the value derived above, 4.9μ, when both magnet and test point are touching the screen.

The demagnetisation effects in the spherical solution also appear in this geometry. For this purpose the appropriate z is the distance from the magnet to the screen. For $z \ll t$ the field in the superconductor is increased by a factor $2/(1+\mu)$. For small t the factor is $1/\mu$ for small s and $2z/t$ for large s. A reasonable approximation is a factor $1/(\mu + t/2z)$. Thus thin sheets can be driven beyond H_m even if the field was much less than this before the screen was inserted.

5. Screening of coils

A common arrangement for detecting superconductivity is to insert a sheet of the material between two thin coils and measure the mutual inductance between them. The argument used to justify a series of images is valid for coils as well as charges, but the values of mutual inductance are more difficult to calculate and another variable, the ratio of diameter to spacing, is involved.

The set of primary coils seen by the secondary is derived from the series in equation (1). If the sheet is of thickness t and the coils are z apart it consists of coils of strength $(1-\beta^2)$, $\beta^2(1-\beta^2)$, $\beta^4(1-\beta^2)\cdots$ situated at z, $z+2t$, $z+4t\cdots$ respectively. Values of mutual inductance can be obtained from reference [4] and the series summed numerically for any particular case. We summarise the general conclusions here.

Firstly, if the spacing of the coils is large compared with their radius they behave as two magnetic dipoles and all the results of the earlier sections can be used. If the coils are close compared with their radius, the inductance of the image coils does not change much until they are further apart than their radius. The number of terms for which this holds in the series of equation (1) is of order r/t where r is the coil radius. If we cut off the series at this point, the field is reduced by $1-\beta^{2n}$ where $n \simeq r/t$, but with a minimum value of 1. This works for both small values of β and for $\beta \simeq 1$. In this latter case $\beta \simeq 1 - 2\mu$ and the field is reduced by $\mu r/t$. This fits in with previous geometries if the relevant size in the screening factor is the coil radius.

These results apply to an infinite sheet, and sheets of a diameter comparable to the coil diameter require more detailed analysis.

The general conclusion to be drawn is that a material made up of individual superconducting grains is not a very effective screen. Firstly the permeability must be very close to zero if the screen is to be thin compared with the dimensions of the screened space. Secondly, if good screening is achieved by a thin sheet it follows that the value of H is greatly increased in the material so that the magnitude of field that can be screened without driving the material over the peak in the magnetisation curve is very small.

Experiments on levitation are normally carried out with rather thick sheets. The magnitude of the image magnet becomes small if s becomes small (the relevant distance z is from the magnet to the sheet), and for $s = 1$ the image strength is about $\frac{1}{3}$ of the levitated magnet. Most levitation takes place at distances comparable with the thickness of the superconducting layer, so quite high permeabilities are tolerable. Films under 10 μm are unlikely to cause levitation without transport currents being carried. Only very small magnets could get close enough and then the high field near the pole pieces will drive the film beyond H_m.

6. Screening using transport currents

If the currents can be carried over macroscopic distances these will provide much more effective screening. The current densities required can be calculated easily in the situations above. For example a current of $I \sin\theta$ A m^{-1} flowing in a spherical shell produces a uniform field inside of $2I$ A m^{-1}. Hence to screen out a field of H_0 we need a maximum current $1.5H_0$ A m^{-1} so the current density is $J_c = 1.5H_0/t$ where t is the screen thickness. In general a field of H_0 can be screened by a screen of thickness t where $J_c t \simeq H_0$. However the very rapid variation of J_c with H_0 in high-T_c superconductors leads to an effective limit on the field that can be screened.

While the current density is dominated by normal barriers it will vary approximately exponentially with field. Suppose $J_c = J_{c0}\exp(-H/H_A)$ where H_A is a constant dependent on the nature and thickness of the weak links. Then if we consider the field distribution across a slab of superconductor parallel to the field

$$dH/dx = J_c = J_{c0}\exp(-H/H_A)$$

if $H = 0$ at $x = 0$ the solution is

$$J_{c0}x = H_A[\exp(H/H_A) - 1].$$

This means that for fields greater than H_A the thickness of the screen rises exponentially so that the effective limit for screening is H_A. This is also the maximum field that can be generated in a magnet wound with wire of the same material. Thus for practical applications to magnets the most important parameter is not the zero-field critical current density, but the field at which J_c falls to about half this value.

Acknowledgments

I would like to thank the US Army for helping to support this work.

References

[1] Josephson B D 1966 *Phys. Rev.* **152** A211
[2] Campbell A M and Evetts J E 1972 *Adv. Phys.* **21** 199
[3] Smythe W R 1968 *Static and Dynamic Electricity* (New York: McGraw-Hill) p 192
[4] Grover F W 1973 *Inductance Calculations* (Research Triangle Park, NC: Instrument Society of America)

Appendix VI

Theory of Currents in Barriers

Paper in Superconductor Science and Technology

Supercond. Sci. Technol. 2 (1989) 287–293. Printed in the UK

Critical currents of barriers in high-T_c superconductors

A M Campbell
IRC in Superconductivity, West Cambridge Site, Madingley Road, Cambridge CB3 0HE, UK

Received 2 May 1989, in final form 17 July 1989

Abstract. Solutions of the Ginzburg–Landau equations are found for three types of barrier which could be the cause of low current densities in high-T_c superconductors. Since the depairing current of bulk material is so much higher than the critical current densities observed, the effect of the barrier on the Ginzburg–Landau parameters must be large to explain the magnitudes of the currents. However, the variation of critical current with temperature shows a large drop well below T_c, which may explain the region of relative reversibility often seen below T_c, and with suitable parameters the critical current drops rapidly with grain boundary angle as observed experimentally.

1. Introduction

The most characteristic feature of high-T_c superconductors is the low value of their critical current densities. The Ginzburg–Landau equations have been remarkably successful in predicting the properties of superconductors, and even when used in regimes beyond their theoretical validity they frequently give qualitatively correct conclusions. In this paper we calculate critical current densities for three types of boundary in a superconductor. The first is a planar defect in a homogeneous material in which the boundary condition on ψ is the same as at a boundary with free space. The second is a barrier in which the superconducting parameters vary smoothly over several coherence lengths, and the third a similar barrier consisting of a dislocation array making up a low-angle grain boundary.

2. The general method

The model used is that of a planar barrier region across which the Ginzburg–Landau material parameters vary smoothly with position. We assume the approximations commonly adopted for weak links, that is to say that the problem is one dimensional, and that the field is small, so that the vector potential, A, can be neglected. This implies that the junction is small compared with the Josephson penetration depth. The current density is then uniform across the junction. We write the order parameter as $\psi e^{i\theta}$.

The Ginzburg–Landau free energy is then given by

$$f_s - f_n = \alpha\psi^2 + \frac{\beta}{2}\psi^4 + \frac{1}{2m^*}\hbar^2\left(\frac{\mathrm{d}\psi}{\mathrm{d}x}\right)^2 + \frac{\hbar^2\psi^2}{2m^*}\left(\frac{\mathrm{d}\theta}{\mathrm{d}x}\right)^2. \tag{1}$$

We assume that the parameters α, β and m^* are smoothly varying functions of position and use the calculus of variations to minimise $\int f\,\mathrm{d}x$ across the boundary. The values of ψ and θ are fixed at large distances from the boundary for a given current so that the conditions for the integral to be a minimum are

$$\frac{\partial f}{\partial \psi} = \frac{\mathrm{d}}{\mathrm{d}x}\frac{\partial f}{\partial \psi'} \quad \text{and} \quad \frac{\partial f}{\partial A} = \frac{\mathrm{d}}{\mathrm{d}y}\frac{\partial f}{\partial \theta'}$$

where $\psi' = \mathrm{d}\psi/\mathrm{d}x$ and $\theta' = \mathrm{d}\theta/\mathrm{d}x$. These lead to the Ginzburg–Landau equations appropriate for spatially varying properties:

$$\frac{\mathrm{d}}{\mathrm{d}x}\left(\frac{\hbar^2}{m^*}\frac{\mathrm{d}\psi}{\mathrm{d}x}\right) - \frac{\hbar^2}{m^*}\psi\left(\frac{\mathrm{d}\theta}{\mathrm{d}x}\right)^2 = 2\alpha\psi + 2\beta\psi^3 \tag{2}$$

and

$$J = \frac{e\hbar\psi^2}{m^*}\frac{\mathrm{d}\theta}{\mathrm{d}x}. \tag{3}$$

Substituting for θ in (2) gives the equation we require to solve for ψ:

$$\frac{\mathrm{d}}{\mathrm{d}x}\left(\frac{\hbar^2}{m^*}\frac{\mathrm{d}\psi}{\mathrm{d}x}\right) - \frac{m^*J^2}{e^2\psi^3} = 2\alpha\psi + 2\beta\psi^3. \tag{4}$$

0953-2048/89/050287 + 07 $02 50

We see that the Ginzburg–Landau equations can be used virtually in their usual form provided we take m^* to be constant.

It is the purpose of this paper to draw essentially qualitative conclusions about the boundaries in high-T_c superconductors so therefore a number of simplifying assumptions will be made to avoid having too many unknown parameters. We shall assume that m^* is constant as the simplest course to take. Other assumptions are unlikely to change the general conclusions.

To make the parameters more physically accessible we put them in terms of physically measurable quantities. These are

$$\xi^2 = -\hbar^2/2m^*\alpha$$

$$H_c^2 = \alpha^2/\beta\mu_0$$

$$\kappa^2 = \frac{m^{*2}\beta}{2\mu_0 e^2\hbar^2}.$$

In what follows the subscript ∞ refers to these parameters in bulk, undamaged, material well away from a boundary. We put

$$J_\infty = \left(-\frac{32}{27}\frac{e^2}{m^*}\frac{\alpha_\infty^3}{\beta_\infty^2}\right)^{1/2}.$$

This is the bulk depairing current, $2\sqrt{2}H_{c\infty}/3\sqrt{3}\lambda$. Also put

$$y = \psi(-\beta_\infty/\alpha_\infty)^{1/2}$$

which is the order parameter normalised to 1 far from the boundary, with zero current flowing. Equation (4) can then be written as

$$\xi_\infty^2 y'' - \frac{4}{27}\left(\frac{J}{J_\infty}\right)^2\frac{1}{y^3} + \frac{\kappa}{\kappa_\infty}\frac{H_c(x)y}{H_{c\infty}} - \left(\frac{\kappa}{\kappa_\infty}\right)^2 y^3 = 0. \quad (5)$$

To reduce the number of possibilities we now assume that the type of damage occurring at boundaries affects mainly the electron–electron interaction, producing an effect similar to raising the temperature. That is, we assume that β is constant and α varies across the boundary. This is equivalent to assuming that H_c is changed while κ remains constant. Once again it is easy to try other variations but qualitative results should be similar.

In terms of the dimensionless quantities

$$x' = x/\xi_\infty \qquad j = J/J_\infty \qquad h(x) = H_c(x)/H_{c\infty}$$

equation (5) becomes

$$y'' - \frac{4}{27}\frac{j^2}{y^3} + h(x)y - y^3 = 0.$$

This is the differential equation that was solved numerically. A barrier symmetric in x was assumed. For large values of y at $x = 0$ the solution diverges, and for small values it oscillates, so various values were tried until a solution was found that did neither of these, up to a distance of five or more times the boundary width. This determined the relative order parameter, y, at the origin to 1 part in 10^{16}.

For $j = 0$ a solution could always be found. For large j, y'' is always positive so the solution diverges. By increasing j from zero until no solution could be found, a value for the critical current density could be obtained. The procedure was not always straightforward since close to the critical current density very small increments in y at $x = 0$ had to be used to avoid missing a solution. However, it was usually possible to determine the critical current to better than 1%.

3. Types of barrier

3.1. Incoherent boundaries

The first type of barrier considered does not involve a continuous variation of the local critical field but takes a uniform material with a modified boundary condition. At a free surface the boundary condition normally assumed is that $\psi' = 0$ but this boundary condition must be changed if ξ is small [1, 2]. The true boundary condition is $\Lambda\, d\psi/dx = \psi$ where Λ is a characteristic distance determined by the effective reduction, or increase, of T_c at the boundary. We assume that this is the boundary condition on ψ at the boundary but that instead of free space or an insulator there is a similar superconductor on the other side of the boundary. In these circumstances ψ will be continuous across the boundary and a current can flow across it.

The variation of ψ is shown in figure 1 for $\Lambda = \xi(T)$, where $\xi(T)$ is the Ginzburg–Landau coherence length. The two graphs show the order parameter for zero current and the critical current. Figure 2 shows the calculated critical current density as a function of $\Lambda/\xi(T)$. The critical current density is normalised to the depairing current density $0.54H_{c\infty}/\lambda$, which is about 10^8 A cm^{-2} at 0 K. The critical current density is roughly proportional to $\Lambda/\xi(T)$ for $\Lambda < \xi(T)$. The

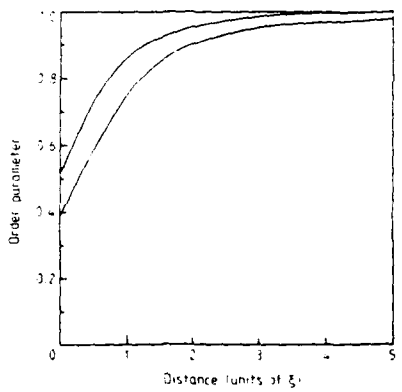

Figure 1. Variation of order parameter with distance from the boundary $\Lambda = \xi$. The two curves are for $j = 0$ and for $j = 0.5$. $j = 1$ is the bulk depairing current and 0.5 the critical current of the barrier

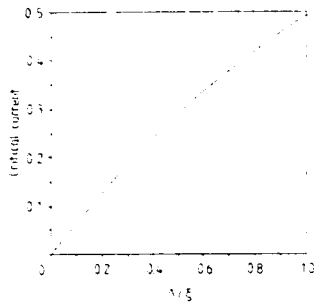

Figure 2. Critical current density as a function of Λ/ξ.

product $J_c\,\xi(T)/\Lambda$ lies between 0.2 and 0.64 for $\Lambda/\xi(T)$ between 1 and 0.04.

3.2. Variation with temperature

The variation of J_c with temperature is due partly to the variation of ξ with temperature and partly to the reduction in the order parameter. The expression for Λ given in reference [1] is $\Lambda = \xi_0^2 T_c\, d/(T_c - T_{cs})$. Here d is the lattice spacing, which we take to equal to ξ_0, and T_{cs} is the critical temperature of the surface region. This is likely to be reduced since diffuse scattering leads to the removal of half the Gorkov kernel. If we suppose T_{cs} is zero so that $\Lambda = \xi_0$ and also $\xi(T) = \xi_0[1 - (T/T_c)^2]^{-1/2}$ with $T_c = 93$ K we can calculate the variation of J_c with T.

Figure 3 shows the result. Since $\xi(T)$ only varies by a factor of four up to 90 K the main source of the reduction in J_c is the reduction in the bulk depairing current, which is reduced by $[1 - (T/T_c)^2]^{3/2}$. This is a factor of 7.7 at 80 K, which is the sort of reduction often observed between helium and nitrogen temperatures.

3.3. Damaged barriers

The second type of barrier considered is the kind of effect produced by a process such as irradiating a short section of a superconducting strip. This was modelled by making α vary as $\{1 - a\exp[(-x/n\xi)^2]\}$. The degree

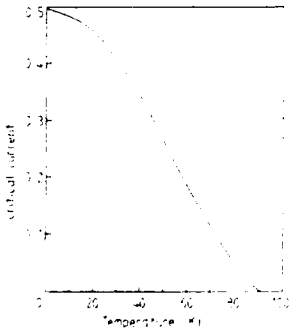

Figure 3. Critical current as a function of temperature for $\Lambda = \xi$.

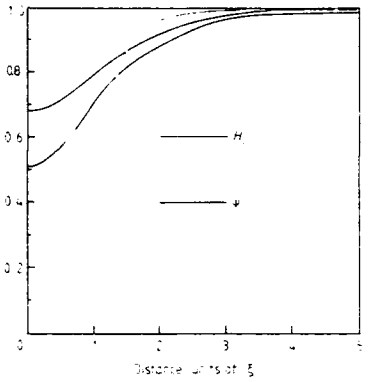

Figure 4. The variation of the order parameter with distance if $H_c = H_{c\infty}[1 - \exp(-x^2)]$. The order parameter is shown for two values of the current, $j = 0$ and $j = 0.5$.

of suppression of H_c at the centre of the barrier is given by a and the width of the barrier in units of the coherence length by n. The boundary condition is now $d\psi/dx = 0$ at $x = 0$. A typical result is shown in figure 4. Here $h = 1 - \exp(-x^2)$, in other words a damaged region of half width ξ where the critical field just reaches zero at the centre. The values are symmetric about the y axis and only positive x is shown. The lighter curve shows the assumed variation in h, i.e. α in the Ginzburg–Landau free energy. The heavier curves show the variation of ψ at two values of j: one is $j = 0$ and the other is $j = 0.5$, the highest current for which a solution could be found.

3.4. Larger barriers

The calculations were repeated for barriers with larger values of a and n, which involves extrapolation of the Ginzburg–Landau theory into material in which α is positive. This is certainly valid for a superconductor not far above its critical temperature and is a plausible hypothesis for material that does not become superconducting even at absolute zero.

The results are shown in Figure 5. This shows the reduction in the depairing current at various values of a for $n = 1$ to 6. We conclude that j_c drops roughly exponentially with both width and depth of the drop in H_c at the boundary. Bands covering the current densities seen in sintered materials (i.e. 1000 A cm^{-2}) and single crystals (300 000 A cm^{-2}) are shaded. These show that in sintered materials the foot of the barrier we are looking for could be, for example, just normal at the centre with a half width of greater than 6ξ, or could be distorted ten times the amount needed to decrease it to normal, over a width ξ.

3.5. Temperature dependence

In order to predict the temperature dependence of J_c we need to know how H_c varies with temperature. We

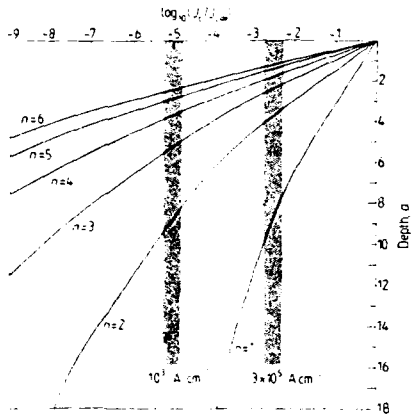

Figure 5. The variation of J_c with width and degree of reduction of H_c. Here $H_c = H_{c\infty}[1 - a\ \exp(-x/n\xi)^2]$

assume

$$H_c = H_c(0)\left[1 - \left(\frac{T}{T_c}\right)^2\right].$$

To use this we also need to know how T_c varies across the barrier, given the variation of H_c. We suppose that the damage reduces α by the same amount at all temperatures, leaving β constant. The variation of H_c with temperature in damaged and undamaged material is illustrated in figure 6. The curve for undamaged material is shifted down by the damage, with the implication that H_c is proportional to T_c^2. Since the temperature is varying we now have to normalise equations to the values at 0 K well away from the boundary, i.e. ξ_0, $H_c(0)$ and $J(0)$. As before, ξ_∞ and $H_{c\infty}$ refer to values well away from the boundary at the temperature of interest. Then

$$\xi_\infty = \xi_0(H_c(0)/H_{c\infty})^{1/2}$$

$$J_\infty = J_0(H_{c\infty}/H_c(0))^{3/2}$$

and

$$H_{c\infty} = H_c(0)[1 - (T/T_c)^2] = H_c(0)(1 - t^2).$$

Putting the distance in units of ξ_0 and substituting $j = J$ normalised by the depairing current at 0 K in

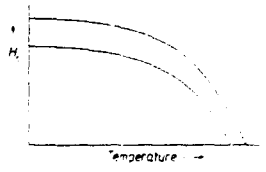

Figure 6. Variation of T_c with H_c (i e x). The upper curve is for undamaged material and the lower for damaged material.

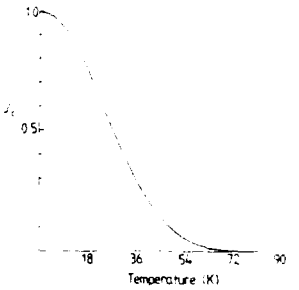

Figure 7. The variation of J_c with temperature if $H_c = H_{c\infty}[1 - 2\ \exp(-x/5\xi)^2]$.

equation (4) gives

$$y'' - \frac{4}{27}\frac{j^2}{y^3(1-t^2)^2} + \left[1 - t^2 - a\exp\left(\frac{-x^2}{n^2}\right)\right]y - y^3(1-t^2) = 0.$$

This equation was solved as before for various values of t and figure 7 shows the results for $T_c = 93$, $n = 5$ and $a = 2$.

The theoretical curve looks a bit like a Gaussian of half width about half T_c. However, over the range 4–50 K it is remarkably linear, extrapolating to zero at around 50 K. Above 50 K the critical current density decays rapidly to very low values. By changing the parameters it is possible to vary the critical current density and the temperature at which it becomes small but the general shape of the curve remains similar. The lower is J_c at 0 K the lower is the temperature at which J_c starts to drop rapidly.

3.6. Low-angle grain boundaries

Experiments by Dimos *et al* [3] have shown that low-angle grain boundaries can cause significant reductions in critical current density, even when apparently quite clean. A low-angle grain boundary is made up of a row of edge dislocations, and outside the dislocation cores, which only occupy a small proportion of the boundary, the main effect is a large linear elastic strain. It is extremely difficult to apply such large strains to bulk samples except under purely hydrostatic conditions so there are few data on the effect of shear strains on T_c. It is plausible that the effect is large, notwithstanding the small effect of hydrostatic pressure. A shear strain of 1 produces essentially a different crystal structure which is unlikely to be superconducting. Within the limitations of a one-dimensional solution we model the effect of a grain boundary as follows. We assume that T_c falls as the square of the strain to preserve the symmetry of the boundary. Since T_c is insensitive to pressure the component of strain used was the von Mises equivalent shear strain. For the results shown the sensitivity to strain was taken to be such that T_c was reduced to zero by a strain of 10%. This would correspond to a stress of

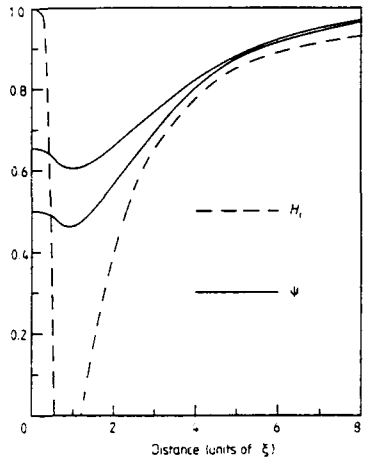

Figure 8. The variation of H_c and ψ near a low-angle grain boundary of 6° inclination if T_c goes to zero at a strain of 10%. The order parameter is plotted for both zero and critical current.

about 4 GPa. The relation between T_c and H_c is taken to be the same as for the disordered grain boundary treated above.

A grain boundary of angle θ has dislocations a distance b/θ apart, where b is the Burgers vector. We take b to be the unit cell size, which is approximately equal to ξ_0. We consider two dislocations at $y = \pm\xi_0/2\theta$, and use the one-dimensional Ginsburg–Landau equation for currents flowing parallel to the x axis. The effect of solving the full problem will be to depress the order parameter on the x axis, where the total shear strain is minimum, and to raise it near the cores due to proximity effect in the y direction. To minimise this effect we look at the currents at a distance 0.8 of the distance from the x axis to one of the dislocation cores. The difference from the two-dimensional solution is unlikely to be as large as a factor of ten.

Figure 8 shows the variation of H_c and the order parameter for a 6° boundary. The lower order parameter is for the critical current which is 0.27 of the bulk depairing current. Figure 9 shows the critical current

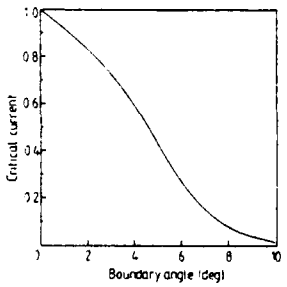

Figure 9. Critical current as a function of grain boundary angle.

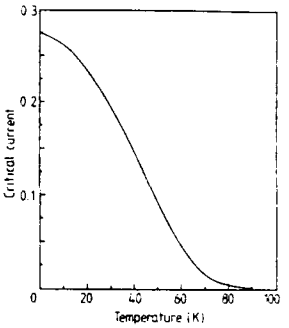

Figure 10. Critical current as a function of temperature for a 6° boundary.

density as a function of grain boundary angle. Figure 10 shows the critical current density as a function of temperature. The critical current density of the complete boundary could be obtained by repeating the solutions for values of y between the dislocation cores and averaging, but in view of the other approximations made we have not done this. A full solution would require a two-dimensional variation of J to optimise the current distribution.

4. Discussion

The main conclusions to be drawn from these results are qualitative. The first comes from the regime in which the Ginzburg–Landau equations are known to be accurate. This is close to T_c and with barriers that are fully superconducting at absolute zero, even if the centre may be normal at temperatures close to the bulk T_c. The general result is that for all three types of barrier the most plausible assumptions lead to current densities much higher than those observed. This is because we are looking for a reduction from the depairing current of the order of 10^5 for sintered material and this requires very large changes in the Ginzburg–Landau parameters.

Where the reduction is due to the boundary condition J_c is reduced roughly in proportion to Λ so that we need values of Λ of the order of $10^{-5}\xi(T)$. If the surface T_c is zero Λ is the order of ξ_0 so there is a major discrepancy here. Continuous barriers must be wide to reduce the current density to experimental values. A barrier in which α varies as $1 - 2\exp(-x/6\xi)^2$ is normal over a distance 8ξ. This has a critical current density of 10^4 A cm^{-2}, which is within the general range observed. It seems doubtful that clean boundaries could cause such disruption, and it suggests that impurity segregation at grain boundaries is causing the low current densities. Similarly the sensitivity of T_c to shear strain must be much larger than to hydrostatic strain if the results are to be explained by this mechanism.

It is possible that our estimate of the depairing current is too high. If we disregard the absolute magni-

tudes then the general form of the current density variation is in agreement with a number of experiments. The variation of J_c with temperature shown in figure 7 was similar over many orders of absolute magnitude in J_c. The striking feature of the curve is the way J_c behaves rather linearly but extrapolates to zero at about half T_c, instead of to T_c itself as tends to happen with flux pinning models. The connection of this with new concepts introduced to explain the magnetic properties of high-T_c superconductors is discussed below.

The variation of J_c with grain boundary angle shows a drop of a factor of ten for an 8° grain boundary. This is in qualitative agreement with the experimental results of Dimos *et al* [3]. However, to obtain this result a number of approximations were made which are likely to underestimate the critical current density and the results were still two orders of magnitude greater than observed. In fact these experimental results contain features that will be difficult to explain on any model. We expect the grain boundary to affect the critical current when its current density drops below that determined by pinning centres. This would lead to an initial range of grain boundary angles that had no effect on J_c since the bulk pinning limit was reached first within the grains, but this was not observed. Also pinning current densities within grains should be independent of grain boundary current densities but a close correlation was observed. It is clear that more experiments are required to clarify the situation.

The approximation used does not allow for any variation of J_c with magnetic field since the junctions were assumed to be narrow. However, the critical current of a type II superconductor can be related to the zero-field depairing current, multiplied by one factor to take account of the reduction in mean order parameter and another to allow for less than ideal pinning. Since the critical current of a broad tunnel junction will depend on the pinning of Josephson vortices we expect the same to apply and the critical current in a field will be closely related to the depairing current in zero field.

5. Relevance to alternative models

The experimental results on high-T_c superconductors have led to a number of suggestions for new models to describe their behaviour. This may be partly due to the fact that a large number of experiments have been made as a function of temperature, while most experiments on conventional type II superconductors have been done at constant temperature. This has obscured the considerable similarities between them. Another complication is that in many, and possibly all, regimes even single crystals of high-T_c superconductors display two sets of properties. One is associated with boundaries, the other with the ideal crystallites. Each has its own H_{c1}, T_c, J_c and H_{c2}. It is rare for a wide range of experiments to be done on the same sample so that no consistent picture has emerged. A recent review by Malozemoff [4] shows these inconsistencies clearly.

Let us first consider the connection between the weak links calculated in this paper and flux pinning. A number of authors have pointed out that there is no sharp dividing line between Abrikosov vortices in bulk materials and Josephson vortices in boundaries [5, 6]. Identical phenomena in the two systems have been described in quite different ways because artificial Josephson junctions have very low current densities and J_c drops rapidly at fields comparable to H_{c1} in type II superconductors. The result is that completely separate regimes of field and current are involved. However, in high-T_c materials we appear to have a range of barriers which vary in their properties from something close to a typical tunnel barrier to something with a current density of 10^5 A cm^{-2} in a field of 5 T. We therefore expect to have to use models based on Josephson junctions, such as the spin-glass model [7], up to fields not previously associated with Josephson junctions. By the same token, models based on flux pinning should work down to very low fields provided we use parameters appropriate to the junctions rather than the bulk material. It is therefore not surprising that no experiment has distinguished between the spin-glass model and the flux pinning model. They are alternative formulations of the same phenomena.

What the experiments do seem to show is a much more rapid decrease in J_c with field and temperature than is observed in conventional superconductors. This is seen in a number of experiments such as the sudden appearance of magnetic reversibility at a certain field or temperature. It is now fairly clear that the reversibility and large Meissner effect in high-T_c superconductors is due to the small size of the current-carrying regions rather than low pinning, and any increase in reversibility might be due to a change in the size of the current paths rather than a change in pinning force. However, the variation of depairing current with temperature in figure 7 does show a very rapid decrease in J_c at about half T_c, which is consistent with a 'reversibility line' [7].

As Malozemoff has pointed out [4], this reversibility line varies with frequency and sensitivity, so it is far from a well defined quantity, but it is worth considering two other explanations that have been proposed for it. It has been suggested that 'flux lattice melting' is an explanation [8]. This supposes that the shear modulus of the vortex lattice is small, leading to an amorphous lattice. Such lattices have been observed in conventional superconductors at low fields. However, all theories of flux pinning predict a large increase in J_c as lattice rigidity decreases and there is a good deal of experimental evidence to show that this is the case [9], so flux lattice melting does not seem a very likely explanation of reversibility.

A more plausible explanation of reversibility is rapid flux creep. The potential pinning flux lines, U, is much greater than kT in conventional materials but the small coherence length and higher temperature raises the possibility that U is of the same order as kT in high-T_c materials. The result of this would be flux flow proportional to the driving force so that the material would

behave as a linear resistor. An effect of this kind is seen in the broadening of the resistive transition when a magnetic field is applied, and this has been explained by Tinkham [10] with a calculation of the energy well in perfect single crystals.

Both these models imply that above the reversibility line the critical current is zero in the same way that the shear strength of a liquid is zero. The most sensitive way of detecting true reversibility is the susceptibility transition in a magnetic field. A reversible type II superconductor is slightly paramagnetic between zero and T_c so that no diamagnetic transition is observed, although this has only been seen in very reversible material of low κ value [11]. Any diamagnetic transition is due to pinning effects. The midpoint is where the pinning penetration depth is of the same order as the particle size so that in high-T_c superconductors it bears little relation to H_{c2} [12]. It will depend on grain size, pinning strength and frequency (because of the viscous drag on flux line movement). The theoretical paramagnetic susceptibility is $1/2\kappa^2$ and so very small, but a true reversibility based on linear flux creep would mean that the diamagnetic transition would not begin until the resistance was zero. Even a small diamagnetic signal above the reversibility line means that the flux creep explanation of resistance cannot be a bulk effect. A network of junctions separating stronger pinning material leads to a diamagnetic signal at T_c, provided J_c is not exceeded by the oscillating external field. Since this would lead to large amplitude-dependent non-linearity, experiments reported are usually below this limit, so that we expect that the diamagnetic transition would be broadened but the start would indicate H_{c2}. On the other hand reversibility due to flux creep would mean that the diamagnetic transition would not start at H_{c2} but would begin when $U \simeq kT$. Measurements of the diamagnetic transition would therefore show a drop in the onset on application of a field. This has been seen in BiSrCaCuO [13] at the very low field of 15 mT but it is hard to reconcile this model with the very high current densities observed at high fields in thin films if bulk flux creep is so fast at 15 mT. Measurements on YBaCuO show only a 10° change in the onset of diamagnetism at 5 T [14] which is more consistent with a genuine variation of T_c with field.

Although the temperature variation of J_c in a proximity effect barrier may be enough to explain reversibility near T_c there is a level of critical current below which flux creep will eliminate irreversibility at low frequencies. The energy barrier for flux crossing a junction is $i_c \varphi_0$ and this can be used for the activation energy in the theory of flux creep. For rapid flux creep $U = kT$, which gives a critical current of 0.5 μA, at 80 K. In sintered material with grains 5 μm in diameter this occurs at a current density of 2 A cm^{-2}, which suggests that rapid flux creep is associated with very imperfect boundaries. If the current density of the boundary is raised to useful values the flux creep should cease to be a problem.

6. Conclusions

With suitable values of the Ginzburg-Landau parameters the critical current densities of several types of boundary can be predicted. To explain the values observed, very large changes in the parameters from their normal-state values are needed. Although this is not impossible in clean materials it suggests that compositional variations may play a major role in lowering J_c. The variation of J_c with temperature may be sufficient to explain the 'reversibility line'.

Acknowledgments

I would like to thank Dr J R Waldram and Dr J Wheatley for a number of helpful discussions. I would also like to thank the Central Electricity Research Laboratories and the European Office of US Army research for supporting the experimental work which stimulated this paper.

References

[1] Deutscher G and Müller K A 1987 *Phys. Rev. Lett.* **59** 1745
[2] Bulaevskii L N, Ginzburg V L and Sobyanin A A 1988 *Sov. Phys.-JETP* **68** 1499
[3] Dimos D, Chaudhari P, Mannhart J and LeGoues F K 1988 *Phys. Rev. Lett.* **61** 219
[4] Malozemoff A P 1989 *IBM Res. Rep.* RC 14267 (to be published in *Physical Properties of High Temperature Superconductors* ed. D M Ginsberg (Singapore: World Scientific))
[5] Martinoli P 1978 *Phys. Rev.* B **17** 1175
[6] Campbell A M 1987 *Proc. LT18 (Japan. J. Appl. Phys.* **26** Suppl. 26-3 2050)
[7] Müller K A, Takashige M and Bednorz J G 1987 *Phys. Rev. Lett.* **58** 1143
[8] Gammel P L, Schneemeyer L F, Waszczak J V and Bishop D J 1988 *Phys. Rev. Lett.* **61** 1666
[9] Pruymboom A, Kes P H and Veen A V 1985 *Proc. Int Symp. on Flux Pinning (Fukuoka)* ed. T Matsushita *et al* (Fukuoka: Matsukuma) p 83
[10] Tinkham M 1988 *Phys. Rev. Lett.* **61** 1658
[11] van der Klein C A M, Kes P H, van Beelen H and de Klerk D 1974 *J. Low Temp. Phys.* **17** 295
[12] Campbell A M 1971 *J. Phys. C: Solid State Phys.* **4** 3186
[13] van den Berg J, van der Beek C J, Kes P H, Mydosh J A, Menken M J V and Menovsky A A 1989 *Supercond. Sci. Technol.* **1** 249
[14] Küpfer H, Apfelstedt I, Schauer W, Flükiger R, Meier-Hirmer R and Wuhl H 1987 *Z. Phys.* B **69** 159

Appendix VII

Demagnetising Effects on Critical Currents

Accepted by Superconductor Science and Technology

The Effect of Sample Shape on the Measurement of Intergrain Currents in YBaCuO

A.M. Campbell and F.J. Blunt

IRC in Superconductivity, West Cambridge Site, Madingley Road, Cambridge, UK.

Short title: Sample geometry and intergrain currents.

Classification: Critical currents 7460J
Other topics 7490

Abstract

The critical current density in sintered YBCO was found to vary by up to a factor of three in sintered material as the angle between the sample and the applied field was varied. Currents were always perpendicular to the field and the effect is attributed to the demagnetising effect of the sample. By defining H as the external field in equilibrium with a flux density B we can use classical electromagnetism to calculate the demagnetising effect. When J_c is plotted as a function of H or B in the material, rather than the external field, the anisotropy disappears.

Introduction

Polycrystalline sintered samples of the superconductor YBCO exhibit two current paths. The grains have very high critical current densities, of the order 10^5 A/cm^2 at 77K in zero field. They are connected by weak links at grain boundaries in which the critical current density is only of the order 10^3 A/cm^2 in the best polycrystalline ceramic samples. The intergrain critical current density is extremely sensitive to applied field and the sample retains a large diamagnetism even after the critical state of the weak links has fully penetrated the sample. This leads to a significant effective permeability and the effects on the real and imaginary parts of the AC susceptibility have been considered in some detail by Müller (1). The flux profile in a sample subjected to a small AC field at low superimposed DC fields has been modelled by Gomory (2). In this paper we show that in rectangular samples the demagnetising factor can lead to a significant difference between the internal and the applied field. This means that critical current densities are not a unique function of the applied field, but by scaling the field with the demagnetising factor J_c becomes a unique function of local fields, provided these are averaged over regions large compared with the grain size.

Experimental

Samples of YBCO prepared by the powder route were pressed and sintered into solid pellets. From these bars were cut, one 10 x 8 x 2 mm, the second 18 x 7 x 0.7 mm. All measurements were carried out in liquid nitrogen.

J_c in the samples was measured inductively. A sinusoidal field was applied with a drive coil and a search coil round the sample measured the response. A balance

coil was used to cancel the signal at low amplitudes in the superconducting state and the signal measured with a lock-in amplifier as the drive amplitude was increased from zero. The signal produced in the search coil of the same phase as that in the normal state measures the flux crossing the boundary of the sample in each cycle (3). The advantage of this treatment over measurements of the real and imaginary parts of the susceptibility is that the curves are more directly related to the penetration of flux into the sample so that it is not so necessary to postulate formulae and fit parameters. Since the intergrain currents are orders of magnitude smaller than the intragrain currents the signal from the search coil plotted against drive amplitude shows a clear discontinuity in gradient. The discontinuity corresponds to the point at which the flux has penetrated all the weak links to the centre of the sample, and is now beginning to penetrate the grains themselves. The value of the drive field at this point is the field across the sample, and J_c can be calculated by dividing this field by the radius of the sample. The precision of this method is greatly enhanced by differentiating the signal with respect to the drive amplitude and plotting this against drive amplitude (Kupfer,4). A typical plot is shown in figure 1. The change in the slope is easily seen, and this is the point at which intergrain currents have penetrated to the centre of the sample. From this plot we obtain the average critical current of a sample, including self field effects. Self field effects appear as a curvature at the start of the trace and are dealt with in a subsequent paper. They were only present in large samples. The ratio of the gradient in the signal beyond the discontinuity to that when the sample is normal gives the effective volume fraction of normal material, and is used to calculate the effective permeability.

A DC magnetic field up to 12 mT could be applied using a solenoid which enclosed the sample and the AC coils. The sample remained in the same orientation with respect to the AC coils but its orientation with respect to the DC field could be altered at will. Two orientations were chosen. In one the largest dimension of the sample was arranged parallel to the applied DC field, in the other the smallest dimension was arranged parallel to the applied field. The coil arrangements are shown in figure 2. With this geometry most of the current flows perpendicular to the field and across the broad face of the sample. It is this critical current which is measured in both orientations by the AC susceptibility technique.

Results

The measurements of J_c with respect to applied field in the two orientations are shown in figure 3. As can be seen the fall in J_c is much more rapid in the sample when placed with the smallest dimension parallel to the applied field and the maximum difference in J_c is a factor of five. This can be related qualitatively to the demagnetising factors of the two shapes, and the volume into which the flux is able to penetrate. It is known that the flux penetrates between the grains, and we call this effective volume of "normal" material V_f This is illustrated in figure 4. The effective volume of "normal" material was generally found to be around 0.4 of the total sample volume. Although this seems large, it includes the pores in the sample which become accessible to the field once the intergrain currents are broken down in addition to a depth approximately equal to the penetration depth λ round each grain.

Theory

The qualitative origin of this effect can be seen from the simple model microstructure illustrated in figure 4. which consists of cubes of superconductor separated by grain boundaries. In a long rod parallel to the field the field within the boundaries is equal to the external field while the average flux density is reduced in proportion to the volume fraction of the grains. If on the other hand the sample is a slab perpendicular to the field all the flux which passed through the area must now be concentrated in the weak links. The average field B is the external B and the field in the weak link is increased in proportion to the volume fraction of superconductor. This simple model appears to make the quantitative results dependent on the detailed shape of the microstructure. However we show below that the situation is an excellent example of the universality of Maxwell's equations provided we define the fields H and B as averages over appropriate volumes of the material. In this case the appropriate volume is several times the grain size.

Following the treatment of Landau and I ifshitz (5) the flux density B is the average over many grains of the field on an atomic scale. The definitions of H and M, which are clear in ferromagnetic materials (Brown, 6), are not so obvious in superconductors, where individual localised magnetic dipoles cannot be identified. Josephson (7) used

the derivative of the free energy with respect to B, while Evetts and Campbell (8) used the external field in equilibrium with B. The first two definitions lead quickly to the third which is directly related to simple experimental measurements of permeability. The fields so defined obey Maxwell's equations. They can be averaged over any region small compared with the sample size and we shall average over several grains. The relation between B and H follows directly from the flux density in a long cylinder parallel to the field, provided there is no significant penetration of the grains. It will be linear and $B = \mu\mu_0 H$, where μ is the permeability measured directly, but approximately equal to the volume fraction of normal material between grains, ie $B = V_f\mu_0 H$. The usual relations between fields then hold, ie $B = \mu_0 H + \mu_0 M$ and $H = H_0 - nM$ where H_0 is the applied field. The result is illustrated in the critical state of a long rod parallel to the field in figure 5. The critical transport current is dH/dx and the flux density gradient dB/dx. If we plot J_c as a function of applied field we get $J_c(H)$. (In the case of the simple microstructure in figure 4 H is the field between the grains). If we put a slab perpendicular to the field we can find H in the material using the effective permeability and the demagnetising factor. By scaling the applied field by the appropriate factor we should be able to bring the two J_c curves into coincidence.

It is immaterial whether we plot $J_c(H)$ or $J_c(B)$ provided we are aware which it is we have measured. It should also be noted that the term 'internal field' is a vague one and has been used to mean both H and B by different authors. It is not necessary for the field between the grains to be uniform for the treatment to be quantitatively exact.

Using the three relationships between M, H and B above, and eliminating M we get

$$H = \frac{H_0}{1-n(1-V_f)} \qquad (1)$$

where H_0 is the external applied field, and n is the demagnetising factor of the sample shape.

The demagnetising factor varies between zero and 1, and therefore for a typical value of $V_f = 0.4$ H may vary between H_0 and $2.5H_0$. Since J_c is so sensitive to field it is not surprising that that this leads to large changes in the critical curent. The demagnetising factors for a general ellipsoid have been calculated, and curves compiled for differing ratios of the semi-axes (9). Calculation of demagnetising factors for shapes other than ellipsoids of revolution is rather difficult, so in this experiment the bars were approximated to ellipsoids. The first had demagnetising factors 0.1 and 0.68 in the two orientations and the second 0 and 1. The two values of H were then calculated from equation 1 and found to be $1.06H_0$ and $1.69H_0$ for the first, and H_0 and $2.5H_0$ for the second. If the demagnetising effect due to the shape and orientation of the sample is responsible for the differing response to the applied field, the curves should coincide if the field scale in the perpendicular orientation is scaled by 1.69/1.06 in the first sample, and 2.5 in the second. The effect of scaling is shown in figure 6. The curves now coincide, within experimental error.

Conclusions

Geometry of the sample must be taken into account when measuring the effect of applied field in Jc in granular materials. The fall in Jc measured experimentally was shown to be strongly dependent on orientation, and could be explained using the demagnetising factors in the two orientations chosen. The results confirm the general theory of electromagnetic fields in materials which allow Maxwell's equations to be averaged over an arbitrary volume of an in inhomogeneous material.

Aknowledgments

We would like to thank the European Office of U.S. Army Research for their support of this work.

1. Müller K.H., MacFarlane J.C., Driver R., Physica C158 69 (1989)

2. Gomory F., Takacs S., Lobotka P., Frohlich K., Plechacek V., Physica C 160 1 (1989)

3. Campbell A.M., J Phys C 2 1492 (1969)

4. Küpfer H., Apfelstedt I., Flükiger R., Keller C., Meier-Hirmer R., Runtsch B., Turowski A., Wiech U., Wolf T., Cryogenics 28 650 (1988)

5. Landau L.D., Lifshitz E.M., Electrodynamics of Continuous Media .

6. Brown W. F. Magnetostatic Principles in Ferromagnetism, North Holland Publishing Co., Amsterdam.

7. Josephson B.D., Phys Rev A152 211 (1966)

8. Evetts J.E., Campbell A.M. Proceedings of 10th Int Conference on Low Temp Physics, vol IIB (Moscow:Veniti) p 33.

9. Osborn J.A. Phys Rev 67 351 (1945)

List of captions

1. Signal differentiated with respect to drive amplitude plotted against drive amplitude.

2. Orientation of sample with respect to the field and measuring coils in the two cases.

3. Critical current densities of the two samples as a function of field in the two orientations.

4. A simple superconducting composite model.

5. The distribution of H and B with depth for a constant critical current density plotted as a function of field, with the field scaled according to the demagnetising factor.

6. The critical current density for the two orientations as a function of H. For one orientation H is the applied field, for the other the applied field is scaled according to equation 1.

(a)

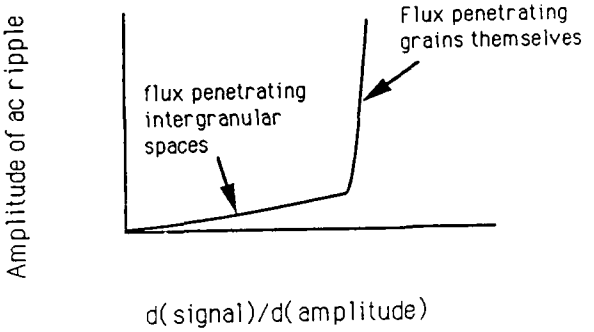
Amplitude of ac ripple
Flux penetrating grains themselves
flux penetrating intergranular spaces
d(signal)/d(amplitude)

Figure 1

Figure 2

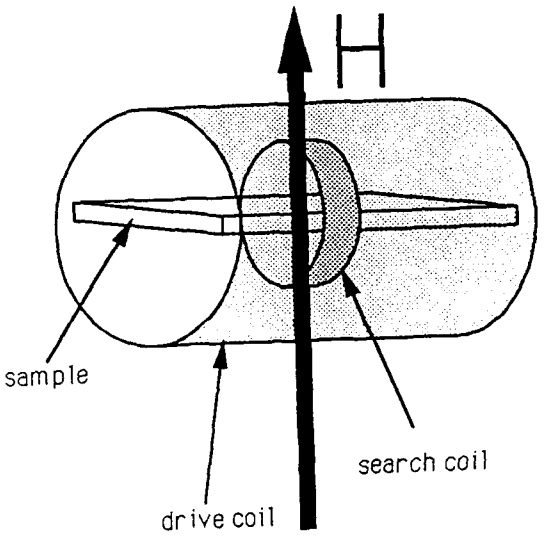
H
sample
drive coil
search coil

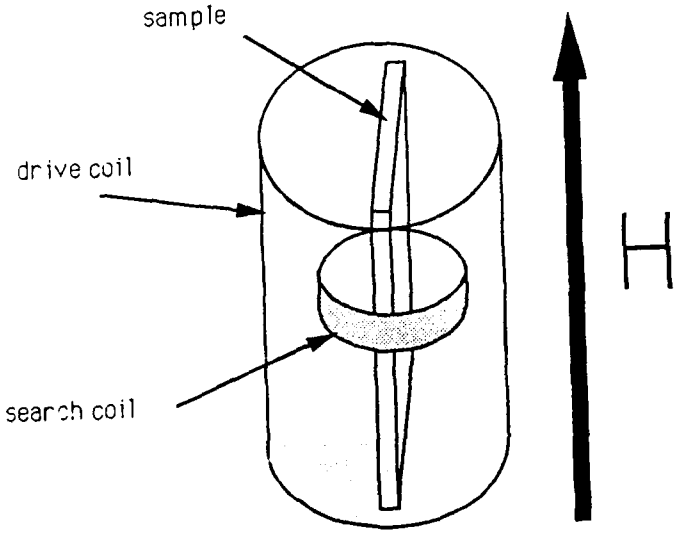
sample
drive coil
search coil
H

Figure 3

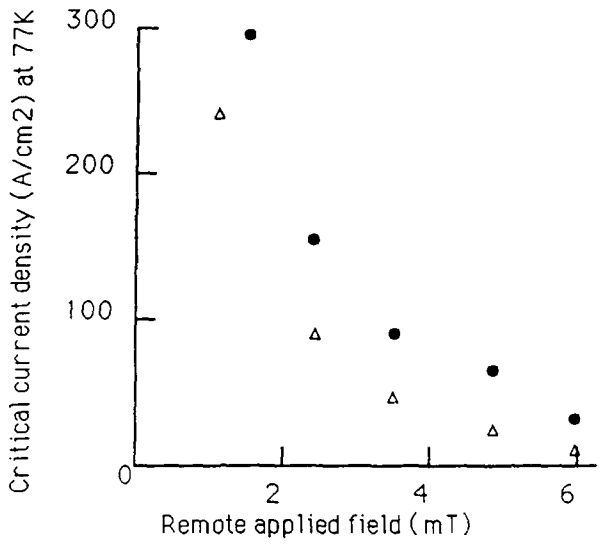

Sample one (10 x 8 x 2mm)

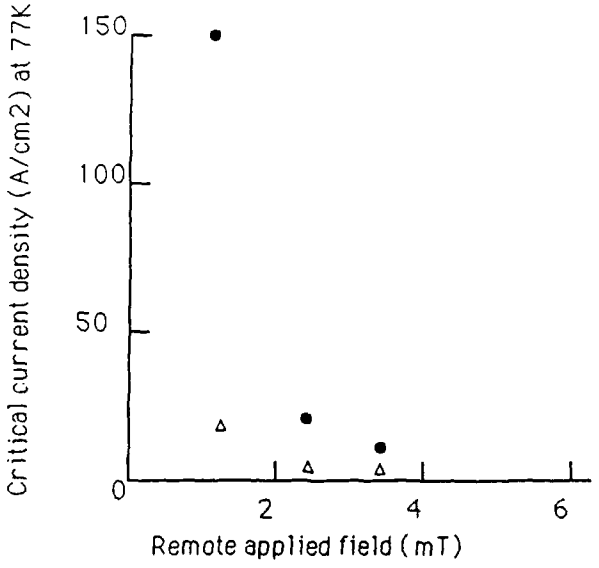

Sample two (18 x 7 x 0.7 mm)

• sample with long axis parallel to the applied field
▵ sample with shortest axis parallel to the applied field

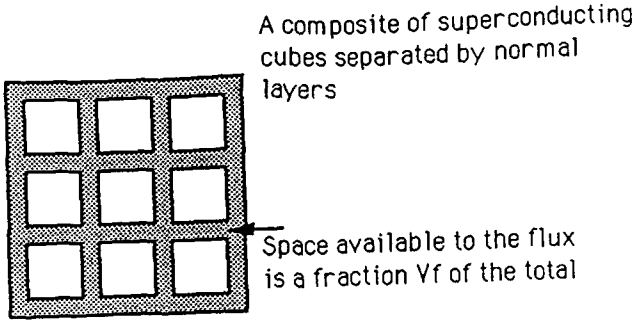
A composite of superconducting
cubes separated by normal
layers
Space available to the flux
is a fraction Vf of the total

Figure 4

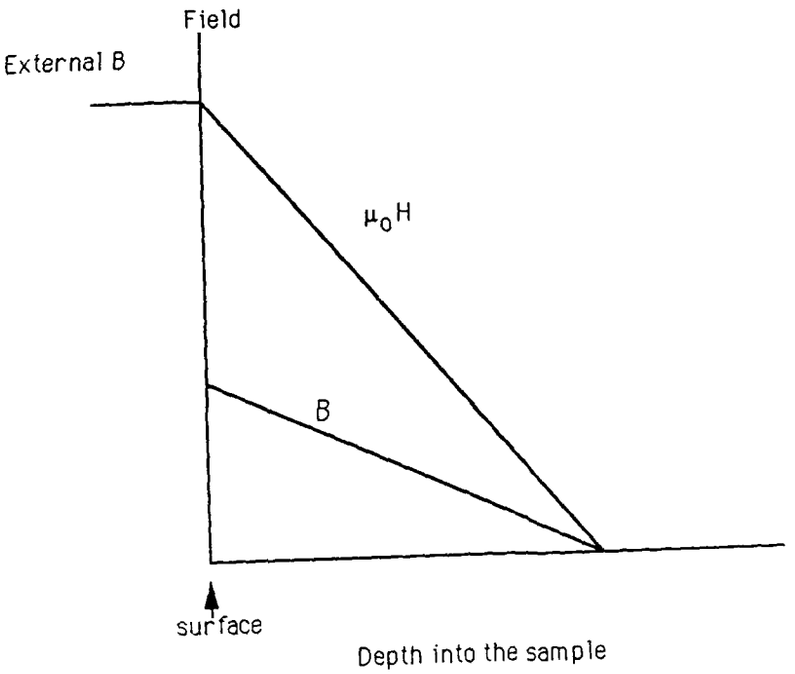

Figure 5

Figure 6

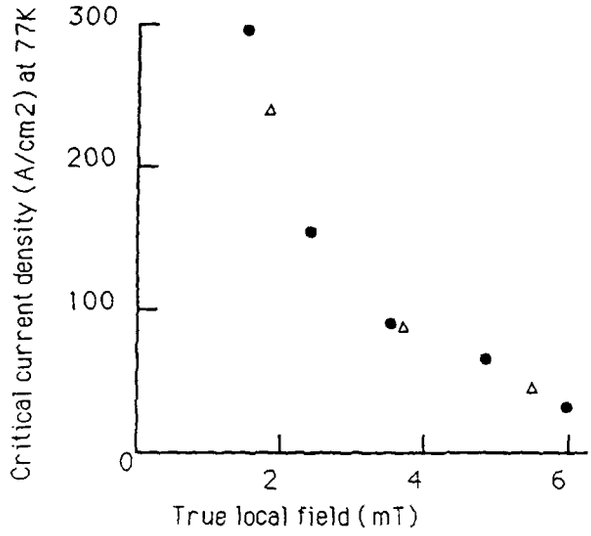

Sample one (10 x 8 x 2mm)

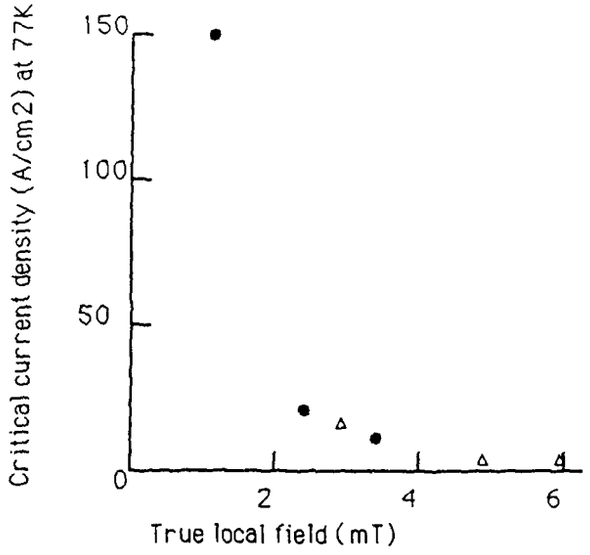

Sample two (18 x 7 x 0.7 mm)

• data for field parallel to long dimension of sample
▵ data for field parallel to shortest dimension of sample, with applied field scaled by the demagnetising factor.